Correspondence to:
S. Volante,
silvia.volante@postgrad.curtin.edu.au;
silvia.volante@rub.de

Structural Evolution of a 1.6 Ga Orogeny Related to the Final Assembly of the Supercontinent Nuna: Coupling of Episodic and Progressive Deformation

S. Volante[1,2,3] , W. J. Collins[1] , A. Pourteau[1], Z.-X. Li[1] , J. Li[1] , and A. R. Nordsvan[1,4]

[1]Earth-Dynamics Research Group, Australian Research Council Centre of Excellence for Core to Crust Fluid Systems (CCFS) and The Institute for Geoscience Research (TIGeR), School of Earth and Planetary Sciences, Curtin University, Perth, Western Australia, Australia, [2]Institute of Geology, Mineralogy and Geophysics, Ruhr-Universität Bochum, Bochum, Germany, [3]ISOTOPIA lab, School of Earth, Atmosphere and Environment, Monash University, Clayton, Victoria, Australia, [4]Department of Earth Sciences, University of Hong Kong, Hong Kong

Abstract The poly-deformed Georgetown Inlier (GTI) in NE Australia has recently been suggested to record a 1.60 Ga orogenic event related to final Nuna assembly. However, the structural evolution of the inlier has remained poorly constrained at the regional scale, and major tectono-thermal events occurred at circa 1.55 Ga. The GTI is the type region for conceptualization of crenulation cleavage development and where the foliation intersection axes (FIAs) approach has been applied. We reevaluated both concepts by combining a multiscale petrostructural analysis with recent petrological and geochronological data. Three main deformation events (D1–D3) and associated composite fabrics (S1–S3) are identified in the GTI. The original NE orientation of 1.60 Ga D1 compressional structures is preserved in the low-grade western domain, and the associated composite S1 fabric is retained as microstructural relicts within circa 1.55 Ga D2 low-strain domains to the east. Extensional D2 structures, characterized by a pervasive, high-grade, composite S2 foliation throughout the central and eastern domains, are interpreted as the footwall of a regional N-S trending, W dipping crustal-scale detachment zone. Syn-D2 S-type granites formed at 1.55 Ga as the detachment evolved. D1 stage was associated with Nuna assembly, whereas D2 represents postcollisional extension. Progressive foliation development occurred twice in the GTI, at 1.60 (D1) and 1.55 Ga (D2), but the previous FIA analysis only records the 1.60 Ga event and cannot be easily reconciled with the regional structural analysis. This study highlights that a multiscale and multidisciplinary approach is required to unravel the structural history of orogenic belts.

1. Introduction

The final assembly of the supercontinent Nuna (Figure 1a) is suggested to have occurred after the collision between Australia and Laurentia (North America) at circa 1600 Ma (Betts et al., 2016; Kirscher et al., 2020, 2019; Pehrsson et al., 2016; Pisarevsky et al., 2014). This orogenic event (i.e., Isan Orogeny) was widely recorded in Proterozoic inliers (Figure 1b) across NE Australia (Betts et al., 2016; Kirscher et al., 2019; Nordsvan et al., 2018; Pehrsson et al., 2016; Pisarevsky et al., 2014; Pourteau et al., 2018). Recent work by Nordsvan et al. (2018) suggested that the oldest sedimentary rocks in the Georgetown Inlier (GTI) were likely sourced from Laurentia and Pourteau et al. (2018) used garnet geochronology and thermodynamic modeling to document simultaneous collisional-type metamorphism in the Mount Isa (MTI) and Georgetown inliers at circa 1600 Ma (Figure 1b). Thus, it was argued that the GTI was an exotic block, sourced from Laurentia, and accreted to the North Australian Craton during the Isan Orogeny at circa 1600 Ma (Nordsvan et al., 2018; Pourteau et al., 2018). However, the structural evolution of the GTI during this collisional event has remained ambiguous, with previous structural investigations focused more on isolated local areas and thin-section scale observations (Bell & Rubenach, 1983; Cihan & Parsons, 2005; Davis, 1995; Duncan & Withnall, 1983). Here we present a detailed reevaluation of regional-scale fabrics and associated metamorphic stages from the GTI to unravel the deformation history related to this Nuna amalgamation event.

In poly-deformed terranes, the variation in mineral assemblages and microstructures associated with successive deformation phases documents the development of fabrics during successive tectonic events occurring
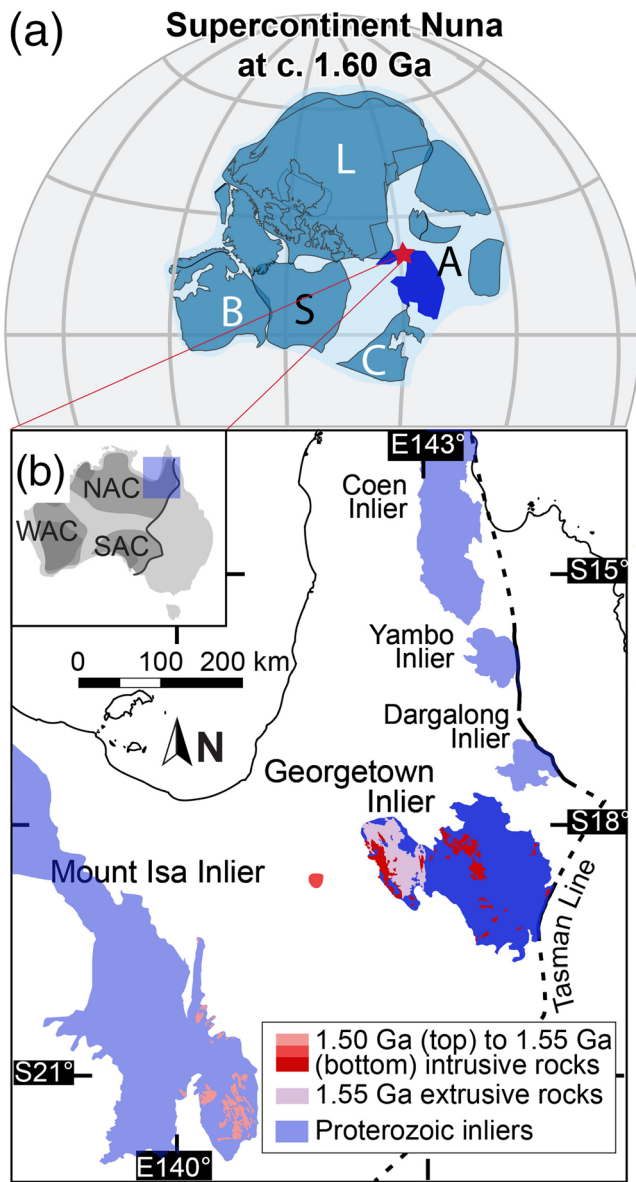
Figure 1. (a) Palaeogeographic reconstruction of the supercontinent Nuna including its core constituent at circa 1600 (adapted after Kirscher et al., 2020). North Australian Craton is marked in darker blue and the red star represents the location of the study area. L—Laurentia, B—Baltica; S—Siberia; A—Australia; C—North China craton). (b) Regional map of the northeast Australian Proterozoic inliers (adapted after Volante et al., 2020). The discontinuous black line "Tasman Line" depicts the eastern margin of the North Australia Craton. NAC = North Australian Craton; SAC = South Australian Craton; and WAC = Western Australian Craton.

under distinct P–T regimes (Connors & Lister, 1995). For this reason, distinguishing between episodic and progressive deformation (intended as continuous deformation) is an essential but challenging task. For decades, structural geologists have combined regional mapping with detailed study of selected outcrops and thin sections to understand the superimposition of multiple generations of structures (e.g., Hobbs et al., 1976; Tobisch & Paterson, 1988; Williams, 1967, 1985; Williams & Zwart, 1977; Withnall et al., 1988; Zucali et al., 2002; Zwart, 1962). Previous local petrographic and structural studies in the GTI have resulted in both simplified (Bell & Rubenach, 1983) and complex (e.g., Cihan & Parsons, 2005) inferred deformation histories. The primary outcomes and controversies associated with previous structural studies can be summarized as follows.

1. Bell and Rubenach (1983) described the microstructural development of the dominant regional fabric phase as progressive deformation during prograde metamorphism. This detailed microscale study focused on microstructural processes and did not address the macroscale structures. The deformation history of the GTI was not placed into a regional context.
2. Cihan and Parsons (2005) inferred bulk shortening directions for the entire GTI from microstructural relationships of foliation intersection or inflection axes (FIAs) in a specific area. They applied the FIA measurement technique (Hayward, 1990) and interpreted the FIAs as representing crenulation hinges and/or intersecting multiple foliations trapped in nonrotating porphyroblasts (Bell et al., 1995). In this model, FIAs are interpreted to record crustal shortening orthogonal to FIAs events, whereas this information is lost in the matrix due to progressively recrystallisation, transpositions, and multiple folding. This approach led to controversial tectono-thermal interpretations in the region (see more details in section 5; Cihan et al., 2006).
3. Previous small-scale structural studies extrapolated the locally identified successive generations of fabrics to the inlier scale, leading to ambiguous tectonic significance (e.g., Cihan & Parsons, 2005; Davis, 1995). More recent metamorphic studies highlighted that the GTI represents a complete crustal section recording collisional and post collisional tectono-metamorphic events at different crustal levels (Volante et al., 2020). In particular, at circa 1550 Ma, the low-grade western domain is juxtaposed to the central and eastern higher-grade domains, which are associated with the emplacement of voluminous S-type granites and extensive migmatization. However, such crustal-scale tectonic contacts were not recognized by previous structural studies. For these reasons, the interpretation that the GTI is a single tectono-metamorphic unit (Withnall, 1996) has never been critically reevaluated.

The deformation history of this poly-deformed terrane requires reassessment at the scale of the inlier. In conjunction with a recent metamorphic study (Volante et al., 2020), a multiscale petrographical and structural (below referred to as petrostructural) analysis was applied to several key areas across the entire GTI to reevaluate (1) the episodic versus progressive deformation concepts, (2) the fundamentals of previous structural interpretations (Bell & Rubenach, 1983; Cihan & Parsons, 2005; Hills, 2003), and (3) the tectonic evolution. The spatial and temporal relationships between local deformation structures were investigated in a regional context and integrated with recent geochronological and petrological results (Pourteau et al., 2018; Volante et al., 2020). We present a new 1600–1500 Ma 3-D structural model for the orogenic event recorded in the GTI marking the final assembly of the supercontinent Nuna (Nordsvan et al., 2018; Pourteau et al., 2018).

Metamorphic domains/ structures		Western domain	Central domain	Eastern domain
D1	*AP1*	N-S striking upright folds	NNE-SSW striking upright folds	
	AX1	moderately SE plunging		
	L1	moderately SE plunging	shallowly NNW plunging	
	S1	steep, N-S striking, ESE-dipping	steep, N-S striking in E-W hinges	
D2	*AP2*		recumbent isoclinal folds	recumbent isoclinal folds
	AX2		dominant ESE plunging, scarse SE-SW-plugnging	NE-SW plunging
	L2		dominant ESE plunging, scarse SE-SW-plugnging	NE-SW plunging
	S2		N-S enveloping surface, shallowly W-dippng	WNW-ESE striking
D3	*AP3*	E-W striking upright open to tight folds	E-W striking upright open folds	E-W striking upright open folds
	AX3	shallowly W-plunging	moderately to shallowly E-W-plunging	moderately to shallowly E-W-plunging
	L3	shallowly W-plunging	moderately to shallowly E-W-plunging	moderately to shallowly E-W-plunging
	S3	E-W striking, sub-vertical	E-W striking, sub-vertical	E-W striking, sub-vertical

Figure 2. Synoptic table of the identified structural elements associated with D1–D3 stages in the western, central, and eastern domain.

2. Regional Geology

The Paleoproterozoic–Mesoproterozoic GTI in north-eastern Australia comprises poly-deformed metasedimentary, metamafic, and granitic rocks, together with nondeformed volcanic and intrusive, felsic rocks. Three main stratigraphic groups of progressively younger age were identified based on detailed lithostratigraphic mapping: the Etheridge (including its lower and upper sequence) Group, the Langlovale Group, and the Croydon Volcanic Group (Figure 2; Withnall, 1996). Unconformities were previously described between these three lithostratigraphic groups (Withnall et al., 2013). The lower part of the Etheridge Group (~1700–1620 Ma; Withnall & Hutton, 2013, and references therein) is interlayered with circa 1660–1650 Ma (Baker et al., 2010; Black et al., 1998) mafic lava flows, dykes, and sills (Withnall, 1985) and likely represents the protolith of the eastern high-grade migmatitic domain (e.g., Einasleigh Metamorphics; Figure 2; Withnall et al., 1988). The upper part of the Etheridge Group was deposited post-1660 Ma, after the mafic magmatism (Black et al., 1998). The entire Etheridge Group was deformed and metamorphosed at circa 1600 Ma during a collisional event (M1) and a second high-temperature M2 event at circa 1550 Ma (Boger & Hansen, 2004; Volante et al., 2020), which was associated with the intrusion of S-type granites, extensive migmatization, and extrusion of comagmatic volcanic units, in the west (Black & McCulloch, 1990; Neumann & Kositcin, 2011; Pourteau et al., 2020; Withnall, 1996).

Recently, a regional metamorphic map of the GTI was constructed (Volante et al., 2020), where metamorphic domains were contoured based on the mineral assemblages that define the most pervasive fabrics at the regional scale. Accordingly, the inlier was divided into *three main metamorphic domains*: (i) the western greenschist facies domain, (ii) the eastern upper-amphibolite to granulite domain, and (iii) the central medium- to upper-amphibolite facies domain.

2.1. Previous Structural Studies

Previous structural studies and their interpretations are presented and discussed below and summarized and compared with this study in Table 1. Many of earlier studies focused on the Robertson River area in the central domain of the GTI, where heterogeneous deformation at different scales allowed the preservation of successive stages of foliation development in adjacent rocks (Bell, 1981, 1986; Bell et al., 1986; Bell & Hobbs, 2010; Bell & Rubenach, 1980, 1983; Reinhardt & Rubenach, 1989). In the Robertson River area, the prograde growth of index minerals was interpreted as progressive, during successive stages of development of the locally dominant foliation (Bell & Rubenach, 1983). This fabric was initially described as the most pervasive foliation in the area, and it was interpreted to be syn-tectonic with the emplacement of S-type granites at circa 1550 Ma. However, such detailed structural studies were not extended to the other domains of the inlier, and the local structural and metamorphic observations were not placed into a regional context.

The view of a dominant progressive deformation event (i.e., D2) associated with continuous prograde metamorphism in the Robertson River area (Bell & Rubenach, 1983) was challenged by Hills (2003) and Cihan et al. (2006), who combined geochronology and metamorphic petrology with structural data and defined four main deformation phases and two main metamorphic events. In particular, Hills (2003) interpreted the oldest, D1 fabric as an extensional foliation developed during the emplacement of mafic sills at circa

Table 1
Synoptic Deformational Classification Schemes for the GTI, Adopted by Previous Authors and Compared With This Study

Black et al. (1979)	Bell and Rubenach (1980, 1983)	Hills (2003)	Cihan (2004) and Cihan and Parsons (2005)	This study
Localities: Robertson River, Percyvale, Einasleigh **D1/M1(?)** **Folds:** tight to isoclinal **Fabric:** S1 slaty cleavage to schistosity **Metamorphism:** prograde **Age:** Rb–Sr 1570 ± 20 Ma **D2/(M2?)** **Folds:** tight to isoclinal **Fabric:** S2 crenulation cleavage to schistosity **Metamorphism:** prograde **Age:** Rb–Sr age of 1487 ± 32 Ma **D3/(M3?)** **Folds:** tight **Fabric:** S3 weak crenulation cleavage/schistosity **Metamorphism:** retrograde **Age:** Rb–Sr age of 969 ± 28 Ma **D4/(M4?)** **Folds:** open **Fabric:** none **Metamorphism:** retrograde **Age:** Rb–Sr age of 400 Ma **D5/(M5?)** **Folds:** open **Fabric:** none	*Localities: Robertson River Synform* **D1** **Macro-scale:** following Black et al. (1979) structural description **Microscale:** S1 relicts in S2 low-strain domains **Metamorphism:** prograde **D2** **Macroscale:** following Black et al. (1979) structural description **Microscale:** six stages of S2 development **Metamorphism:** From St-Grt (stages 1–3 of S2) to And and Sil (stage 4–6 of S2) **Age:** Rb–Sr age of 1487 ± 32 Ma **D3, D4, D5 (not discussed)** **Folds:** not discussed **Fabric:** S3 weak crenulation **Metamorphism:** retrograde **Age:** refer to Black et al. (1979)	*Localities: Stockyard Creek, Robertson River and Einasleigh* **D1/M1** **Folds:** none **Fabric:** S1 extensional layer-parallel fabric, not recorded in the upper Etheridge **Metamorphism:** prograde from W to E **Age:** 1675–1655 Ma **D2** **Folds:** tight to isoclinal, recumbent to inclined (F2) **Fabric:** S2 slaty cleavage to gneissic foliation **Metamorphism:** greenschist to granulite metamorphic grade **Age:** circa 1553 Ma. Followed by Langlovale deposition **D3** **Folds:** inclined tight to open, upright F3 **Fabric:** open crenulation cleavage **Metamorphism:** greenschist to granulite metamorphic grade (W to E). **Age:** 1553–1550 MaRSG **post-D3 and pre-D4** Emplacement of granitoids, dykes and partial melting. Extrusion of volcanic rocks **Age:** 1550–1545 Ma **D4** **Folds:** N-S trending open F4 **Fabric:** none	*Localities: Robertson River synform and antiform system* **Macroscale folding** **Folds:** E-W trending **Fabric:** pre-S1/2 **Metamorphism:** prograde(?) **Age:** 1657–1605 Ma **FIA 1 (ENE-WSW)** **Folds:** none, **Fabric:** pre-S1/2, in garnet core **Metamorphism:** Grt stability field **Age:** not dated, pre-1605 Ma **FIA 2 (E-W)** **Folds:** none, **Fabric:** pre-S1/2, in garnet rims **Metamorphism:** Grt stability field **Age:** 1640–1605 Ma **FIA 3 (N-S)** **Folds:** none **Fabric:** syn-S1/2, in Grt-St **Metamorphism:** midamphibolite facies **Age:** 1610–1580 Ma **FIA 4 (NE-SW)** **Folds:** none, **Fabric:** syn-S3/4, in St	*Localities: (refer to Figure 3)* **D1/M1** **Folds:** NNE trending upright F1 **Fabric:** NNE striking, E dipping composite S1 (S1a and S1b) **Metamorphism:** greenschist facies in the western domain; prograde MP–MT (midamphibolite facies) in the central domain **Age:** Lu-Hf in garnet and U-Pb in monazite 1604-1590 Ma **D2/M2** **Folds:** N trending tight to isoclinal, recumbent F2 **Fabric:** N striking, W dipping, extensional composite S2 (S2a and S2b) high-grade foliation **Metamorphism:** andalusite static overgrowth in the western domain; LP/MP–HT (upper amphibolite to granulite facies) in the central and eastern domain **Age:** U-Pb in monazite at circa 1550 Ma 1604–1590 Ma **D3/M3** **Folds:** E-W trending open to tight, upright doubly plunging F3 **Fabric:** E-W striking, subvertical S3 crenulation cleavage/schistosity **Metamorphism:** greenschist facies to low-amphibolite facies in the western and central and eastern domains, respectively **Age:** post-1550 Ma, likely around 1545-1540 Ma (Hills, 2003) **post-D3 (D4?)** Possible N-S trending F4 folds weakly refolding F3 and generating doubly plunging F3

Table 1
Continued

Black et al. (1979)	Bell and Rubenach (1980, 1983)	Hills (2003)	Cihan (2004) and Cihan and Parsons (2005)	This study
Metamorphism: retrograde		**Metamorphism:** none	**Metamorphism:** St–And stability field	
Age: Rb-Sr age of 300 Ma		**Age:** 1540 Ma (?)	**Age:** 1580–1507 Ma	

Note. Mineral abbreviation after Whitney and Evans (2010).

1660–1650 Ma. D2 structures (ca. 1553 Ma) were interpreted as E-W trending folds, with a regional axial planar fabric associated with staurolite and sillimanite growth in the central and eastern domain, respectively (Hills, 2003). The D2 stage was interpreted by Boger and Hansen (2004) to occur at the same time in the two domains, but at different P–T conditions (600–650°C, 6–7 kbar in the central domain and ~770°C, 8–9 kbar in the eastern domain). At circa 1553–1550 Ma, the development of NW-SE upright folds (D3) was suggested to precede the circa 1550–1545 Ma emplacement of pegmatites, granitoids, and volcanic rocks in the eastern, central, and western domains, respectively (Hills, 2003; Table 1).

Alternatively, Cihan and Parsons (2005) identified four sets of FIAs in the Robertson River area associated with five matrix foliations and additional ones only preserved as inclusions trails in the earliest formed FIA set 1. These authors described the oldest FIA1-2 (D1) deformation phases only as inclusion trails in garnet porphyroblasts. No related fabrics were identified in the field. D1 was interpreted to occur between circa 1655 and 1610 Ma, based on U-Pb chemical dating of monazite, and it was attributed with N-S bulk shortening (Cihan et al., 2006). The D2 deformation phase (ca. 1610–1580 Ma) was ascribed to axial planar fabric (e.g., S1/2 in Cihan & Parsons, 2005) preserved within garnet and staurolite porphyroblasts in the central domain and attributed to E-W bulk shortening. Between circa 1580–1507 Ma, NW-SE bulk shortening was associated with the development of S3/4, which was identified only within staurolite porphyroblasts (Cihan & Parsons, 2005). This final stage was interpreted as the initial decompression and exhumation of the terrain associated with widespread granite intrusions (Cihan et al., 2006; Cihan & Parsons, 2005).

2.2. *P–T* History

Recent results (Volante et al., 2020) attributed the oldest composite fabrics (i.e., S1a and S1b) to progressive shortening at circa 1600 Ma, during prograde burial and heating (M1a), along a medium-P/T gradient and culminated (M1b) in the staurolite-garnet stability field. Metamorphic monazite ages constrain the timing of a subsequent lower-pressure metamorphic overprint (M2) at circa 1550 Ma (Cihan et al., 2006; Volante et al., 2020), with generally increasing peak temperature from the central to the eastern domain. Between M1b and M2a decompression and exhumation occurred followed by an initial thermal overprint (M2a) and subsequent isobaric heating (M2b) (e.g., Cihan et al., 2006; Volante et al., 2020). The M2 event was accompanied by the development of a shallow S2 foliation associated with partial melting and granite emplacement in the eastern and central domain, respectively (Black et al., 2005; Black & Withnall, 1993; Neumann & Kositcin, 2011). Finally, D3 produced E-W trending folds and a retrograde axial planar cleavage (S3) under greenschist facies conditions (M3) post-1550 Ma (Volante et al., 2020). By contrast, Cihan and Parsons (2005) interpreted the E-W trending FIA1-2 as pre-1600 Ma. Ultimately, the lack of structural consistency between the identified four FIAs sets and the macroscopic E-W folds in the Robertson River area, led Cihan and Parsons (2005) to conclude that the E-W folding in this area occurred prior to porphyroblasts growth and the extensive metamorphism, possibly soon after circa 1,655 Ma.

3. Methodology

3.1. Petrographical and Structural (i.e., Petrostructural) Mapping

In Proterozoic poly-deformed terrains such as the GTI, overprinting relationships are found only in specific outcrops, and continuity of structures is nonexistent at the regional scale. For these reasons, it is essential to conduct detailed field work where structural measurements are combined with petrological and lithostratigraphic data (Gosso et al., 2015; Passchier, 1990). Geometric analysis at outcrop scale (or mesoscale) was integrated with constraints gleaned from 1:250,000 and 1:100,000 scale geological maps (Bain et al., 1985; Bain & Draper, 1997). Structural relationships between foliation and bedding were used to determine the lateral continuity of tectonic fabrics when possible. Foliation trajectories (i.e., orientations) were further refined using parageneses, which varied depending on bulk-rock compositions and metamorphic grade. Microstructural analysis was integrated with mesoscale and macroscale mapping to define the relationships between fabrics and mineral growth for each deformation event to deduce the sequence of superimposed structures and to determine the relative chronology between successive deformation events at the inlier scale.

For regional correlations, it is important to subdivide petrostructural observations from the study area in adjacent subareas and associated with each fabric the relative chronological history (Figure 2) and the mineral assemblages. For this reason, macrostructural, mesostructural, and microstructural observations

are presented and combined with detailed structural maps, cross sections and stereographic projections (equal area and lower hemisphere), for representative selected subareas of the western, eastern, and central domains.

Petrographical and structural mapping was carried out, building on published petrological and structural observations and interpretations (e.g., Cihan & Parsons, 2005; Reinhardt & Rubenach, 1989; Withnall et al., 1988). Two field campaigns shed light on the most critical and complex areas (Figure 2). Where the fabric elements are numerous, mapping the foliation trace grid locates the compatible strain domains and the kinematically coherent mosaic of time-related fold sets and its mineral-scale foliations necessary to establish changes in the equilibrium assemblages. In each recently identified metamorphic domains (i.e., western, central and eastern domains in Volante et al., 2020), sets of significant structural measurement may then be differentiated chronologically within subareas. In this scenario, the selection of strategic samples is facilitated by the location of low strain zones, where the structural and metamorphic relicts are preserved.

The low-grade western domain is here divided into four main subareas: Western Creek and Townley Stations, Paddys Station, Stockyards Creek, and Ortona Station (Figure 3). The eastern domain includes one main subarea characterized by a migmatitic complex (i.e., Einasleigh Metamorphics). The central domain is subdivided into two subareas, including the Lornevale/Lighthouse and the Robinhood granitic dome (Figure 3).

In the studied subareas, the following structural elements were measured: dominant foliations or crenulation cleavages (Sn), fold axial planes (APn), mineral stretching lineation (Ln), and fold hinges (AXn) where "n" indicates the generation of the deformation event.

By combining the petrostructural information with previous geochronology data and *PT* estimates (Volante et al., 2020), discrete tectono-metamorphic units (Spalla et al., 2000) are identified.

3.2. Microstructural Analysis

For the microstructural analysis of selected samples, we use porphyroblast-matrix relationships to establish the relative timing between metamorphism and the development of the fabrics (Bell et al., 1986; Bell & Rubenach, 1980, 1983; Passchier & Trouw, 2005). Thin sections of the studied samples were commonly cut parallel to the lineation (when present) and normal to the dominant fabric. Mineral abbreviations adopted throughout the text and figures are from Whitney and Evans (2010), except for white mica (wm). A synoptic representation of microstructural evolution during the successive deformation stages in metapelitic rocks is reported for the western, central, and eastern domains (Figure 4).

4. Structural and Microstructural Analysis

In this section, a summary of the regional deformation history (Figures 2 and 4) is combined with recently published geochronology data and *P–T* estimates to provide the platform for a more detailed macroscale, mesoscale, to microscale structural analysis of overprinting relationships at several key locations.

4.1. Regional Structural Framework

Based on microstructural and metamorphic criteria (Volante et al., 2020), three structural episodes were identified in the GTI: D1 at circa 1600 Ma, D2 at circa 1550 Ma and D3 post-1550 Ma. Also, three main metamorphic domains (western, central, and eastern) were recognized (Figures 2 and 3).

In the western domain, the circa 1,600 Ma regional foliation (S1) is defined by a greenschist facies mineral assemblages (M1). A circa 1550 Ma *LP–MT* overprint during M2a (2–4 kbar; 300–550°C) is characterized by static overgrowth of andalusite (i.e., not associated with the development of any foliation). Later deformation is characterized by regional upright folds with an axial planar crenulation cleavage that varies from NW to W trending and becomes progressively more intensely developed southward. These are described as F3 because they fold a high-grade S2 fabric in the adjacent central domain (see below).

The adjacent central domain records progressive circa 1600 Ma (D1) deformation, defined as S1a and S1b, which developed under prograde *MP*-amphibolite facies conditions (M1 stage; 6–9 kbar and 530–660°C). These fabrics were overprinted during a second metamorphic event (M2) characterized by andalusite
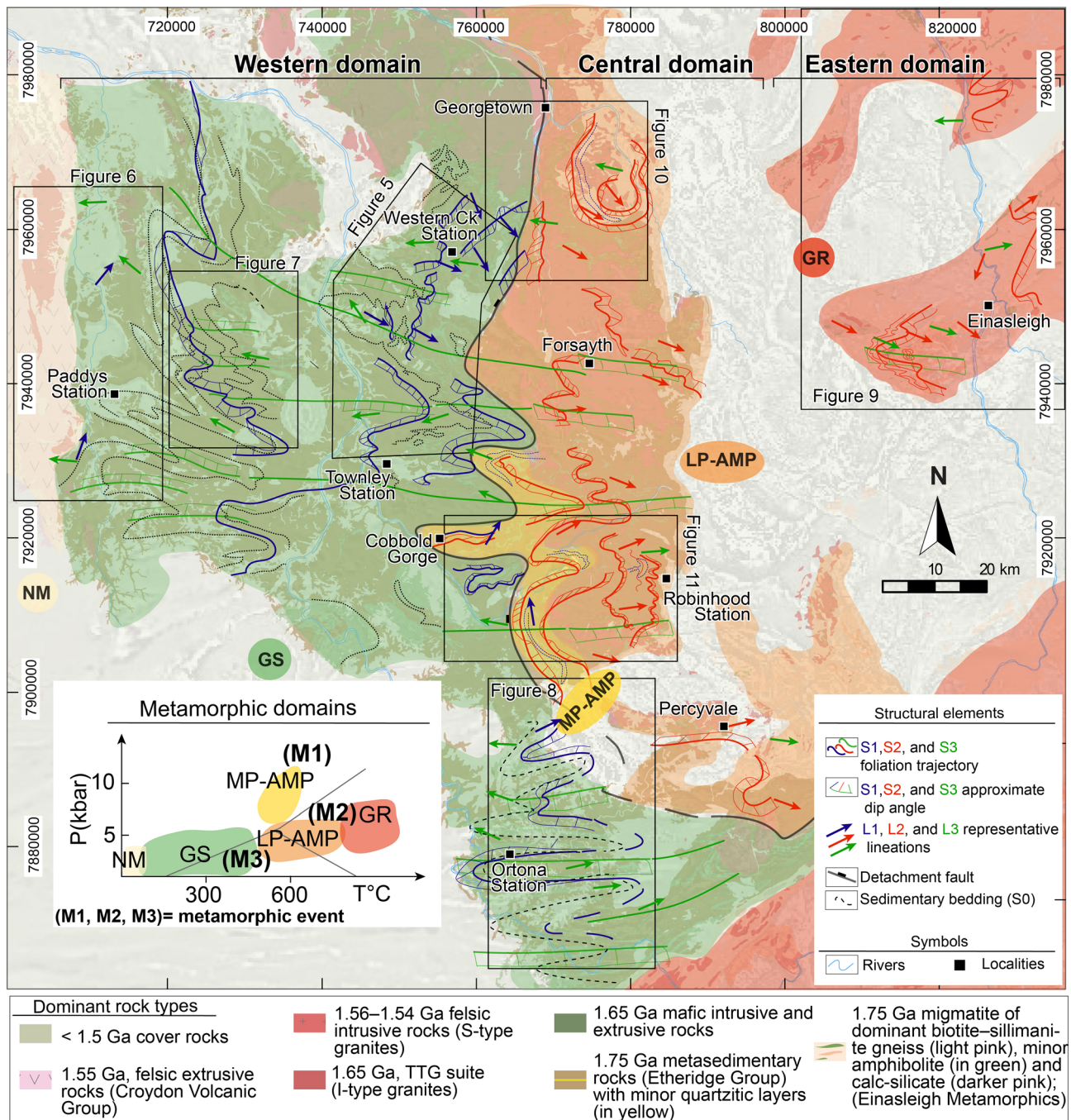
Figure 3. Structural and metamorphic map of the GTI (adapted after Volante et al., 2020). Proterozoic rocks overlay a greyscale mosaic of total field magnetic intensity (TMI) data where the first vertical derivatives (1VD) was applied. Foliation trajectories of the dominant fabric at the regional-scale and associated lineations are represented in a synoptic map. The metamorphic grade colors highlight the western, central, and eastern metamorphic domains (see legend). More detailed figures that cover the key studied localities are enclosed in the black boxes.

(M2a) and sillimanite (M2b) overgrowth on staurolite at circa 1550 Ma, with M2b peaking at 4–6 kbar and 600–680°C (Volante et al., 2020). The dominant regional S2 foliation is defined by sillimanite and biotite and forms a N-S trending, shallow W dipping enveloping surface. This S2 fabric truncates the D1 structures at a high angle in the northern part of the study area (Figure 3), but farther south D1 and D2 structures tend to be realigned into D3 orientations, where F3 folds are more intensely developed.
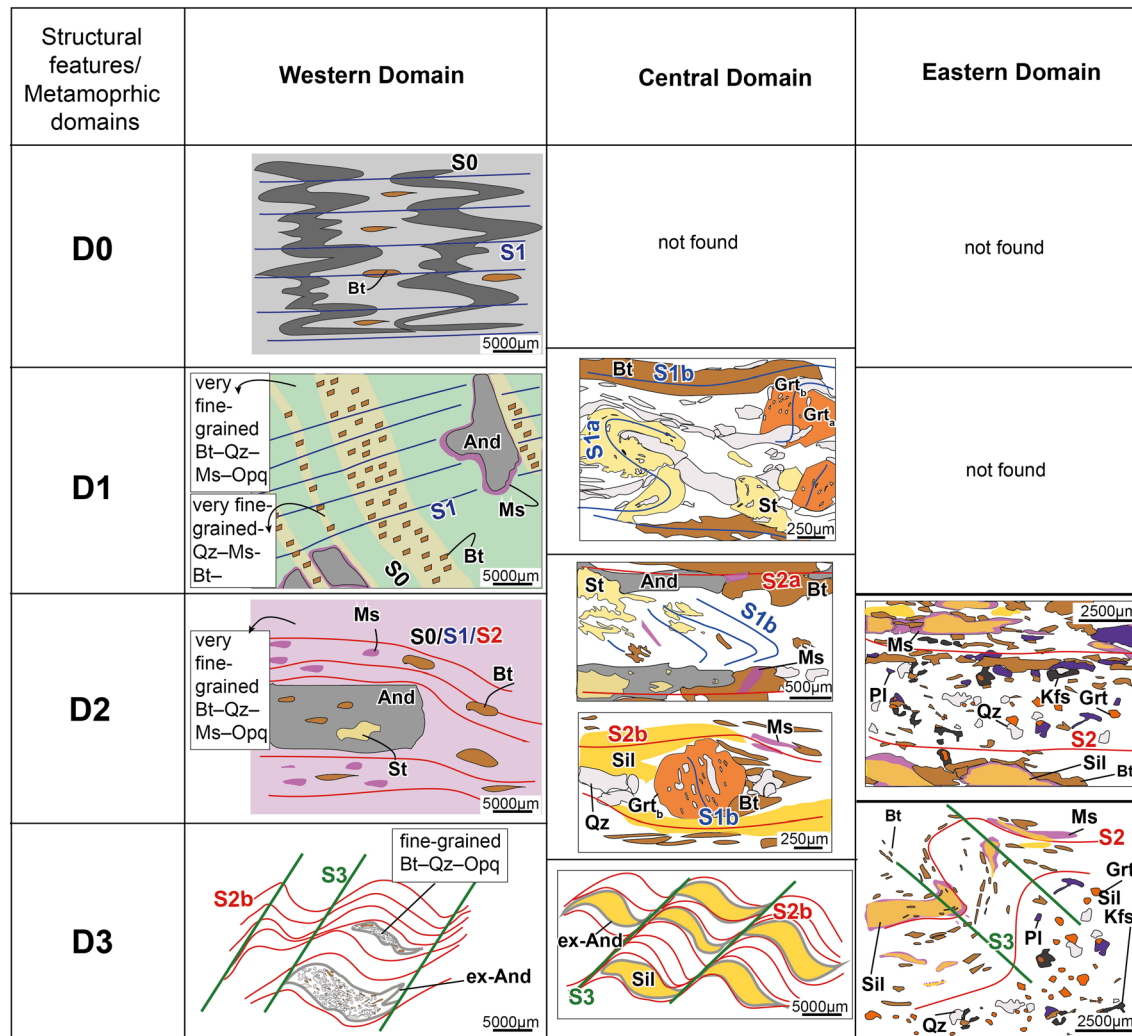
Figure 4. Synoptic representation of microstructural evolution during successive deformation stages in metapelitic rocks of the GTI.

In the eastern domain, no D1/M1 metamorphic and structural record was recognized. The D2/M2 partial melting event is instead recorded at *MP–HT* conditions (~8 kbar and 710–770°C), with peak mineral assemblages formed in the S2 fabric. As with the eastern domain, the dominant S2 fabric of the central domain is the migmatitic foliation. In both domains, this S2 foliation was dated by U-Pb geochronology on monazite at circa 1550 Ma (Volante et al., 2020). This foliation is folded into dominantly E-W trending structures, similar in orientation and amplitude to the F3 folds of the other two domains (Figure 3). Increasing M2 peak pressure from the central domain (4–6 kbar) to the eastern domain (~8 kbar) indicates that the migmatitic complex in the east was structurally below the main emplacement crustal level of granitoids within the central domain.

4.2. Western Domain

This section presents the results of our detailed structural analysis in four subareas (i.e., *Western Creek-Townley Station, Paddys Station, Stockyard Creek, and Ortona Station*) in a series of maps, cross sections, and mesoscale to microscale observations (Figures 5–8).

Area 1: *Western Creek-Townley Station-Western domain* (Figures 5a–5g). Based on the regional structural correlations described above, D1 and D3 structures were identified in this locality.

D1 structures. In the vicinity of *Western Creek* station (Figure 5a), alternations of pelitic and psammitic metasedimentary and metamafic rocks define the bedding (S0). At microscale, S0 is defined by alternations of
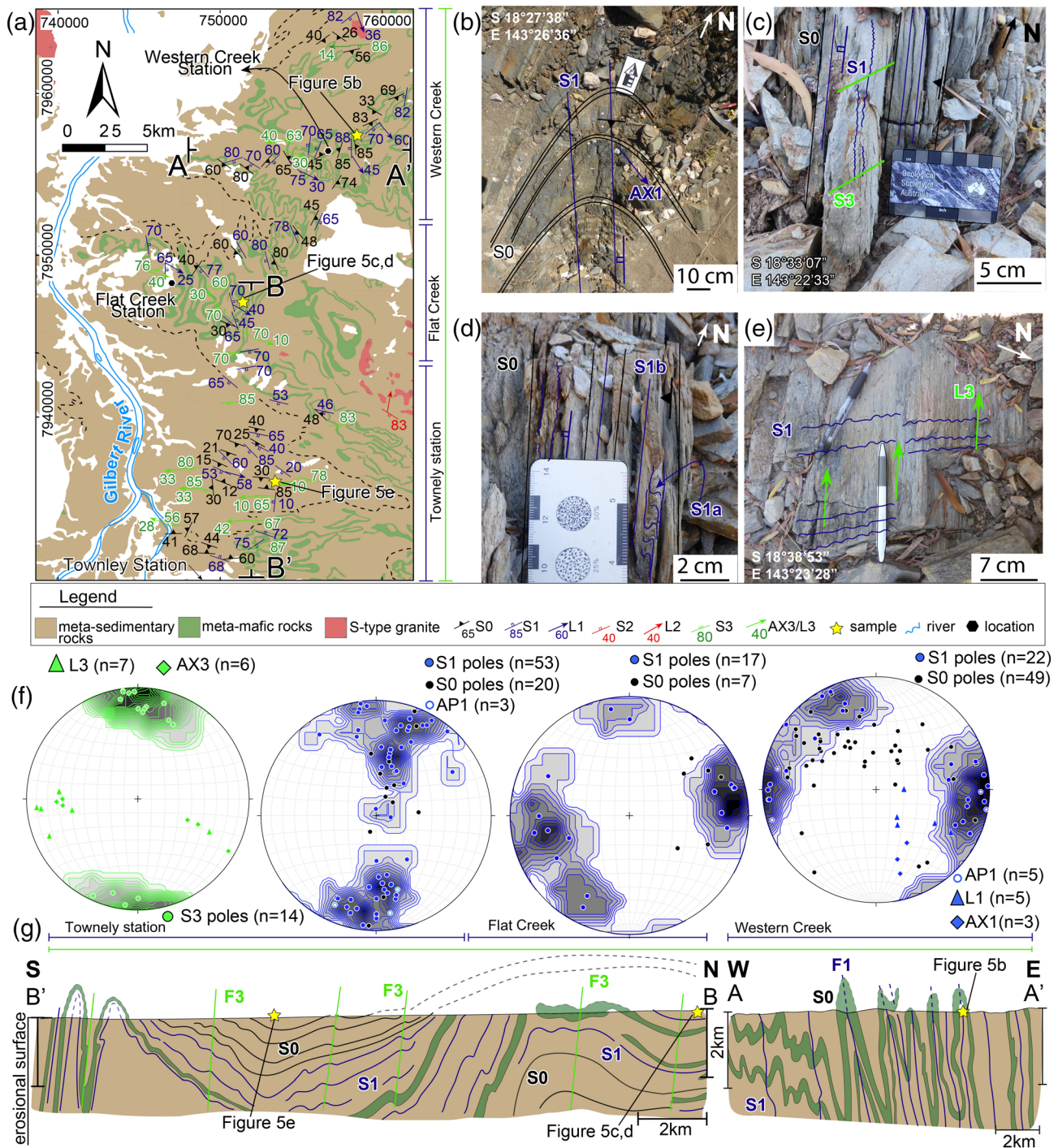
Figure 5. (a) Geological map of the Western-Flat Creek and Townley Stations area with representative structural measurements. (b–e) Field photographs showing the relationships between the bedding (S0), the dominant cleavage (S1) and the younger crenulation axis and lineation (i.e., AX3 and L3). (f) Stereographic diagrams (equal area, lower hemisphere projections) from left to right: density diagram of the S3 poles and related linear structures (e.g., AX3 and L3); density diagrams of the S1 poles, overlain by poles to bedding (S0), poles to F1 axial plane (AP1) and by linear structures (e.g., AX1 and L1); (g) interpretative W-E (AA′) geological cross section of the dominant structures in the Western Creek area and N-S (BB′) cross section of the dominant structures from Flat Creek toward Townley Station.

pelitic (fine-grained biotite + muscovite + quartz) and more quartzitic (biotite, opaques [likely Fe-Ti oxides], and andalusite porphyroblasts) layers. Bedding is folded by the first generation of tight upright folds (F1), trending 170°N and plunging variably (45–70°) to the E-SE (Figures 5b and 5f). These folds are associated
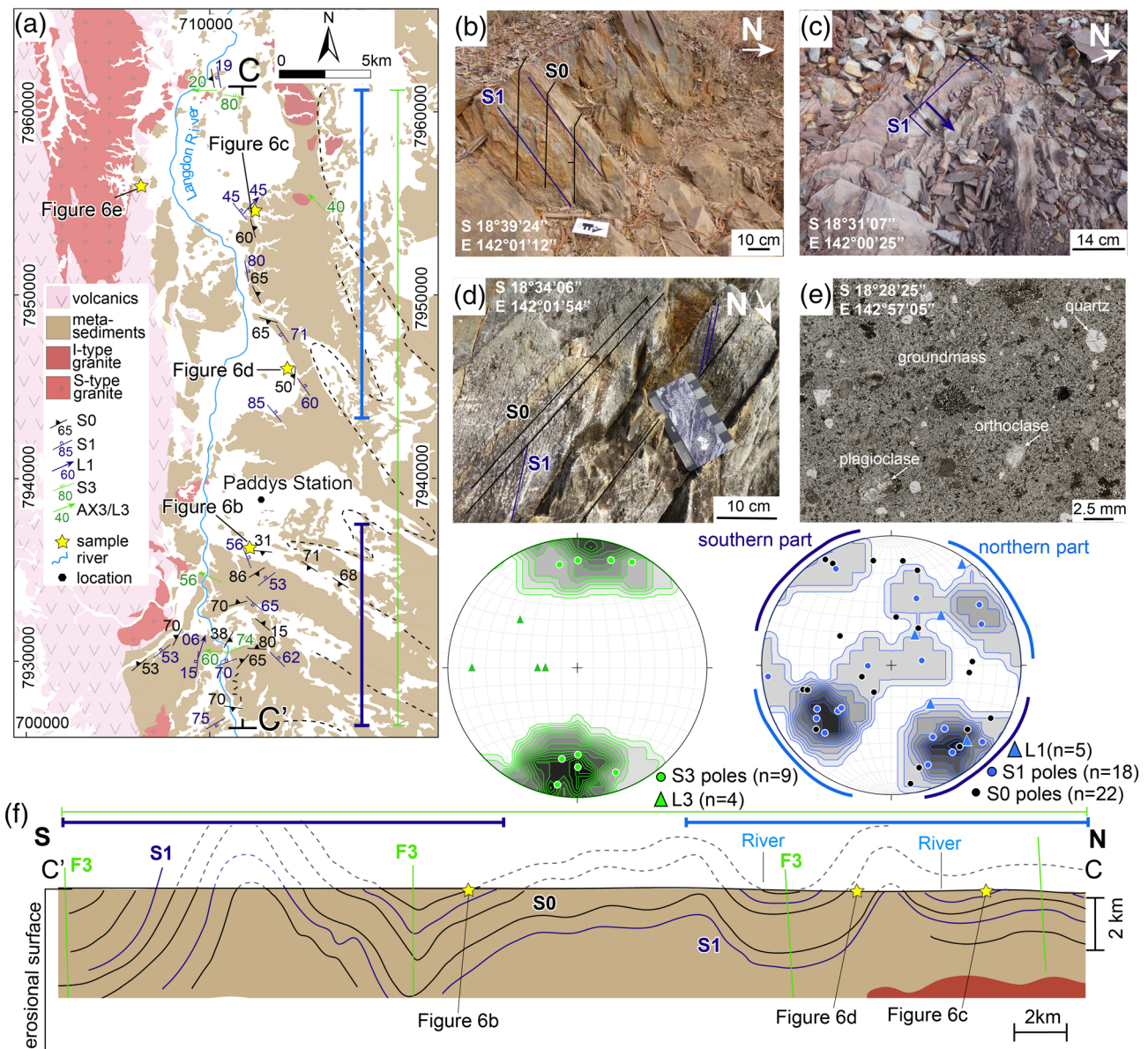
Figure 6. (a) Geological map of the Paddys Stations area in the western domain with representative structural measurements. (b–d) Field photographs showing relationships between the bedding (S0) and the dominant cleavage (S1). (e) Microphotograph (plane-polarized light) of the nondeformed Croydon volcanic rocks. (f) Stereographic diagrams (equal area, lower hemisphere projections) of planar and linear structures and interpretative N-S geological cross section (CC′) of the dominant structures. Density diagrams of the S1 poles (blue) and the S3 poles (green).

with the development of a steep (60–80°), ESE dipping pervasive axial planar cleavage S1 (Figures 5b–5g) defined by biotite shape preferred orientation (SPO) and minor fine-grained quartz–opaque aggregates (Figure 4). It is axial planar (S1) to the observed F1 folds, confirming that it is the first tectonic fabric recorded in this area, that is characterized by a greenschist facies mineral assemblage (i.e., M1 in Volante et al., 2020). Mineral lineation and S0/S1 intersection lineations (L1) plunge southeast, parallel to the F1 fold hinges (Figure 5f). Variations in the orientation of the F1 folds may be associated with complexities associated with D1 structures (see below) and/or may partly result from later deformation.

The dominant NNE-SSW striking S1 fabric can be traced southward to the northern part of *Flat Creek* station (Figure 5a). At this locality, rare intrafoliation isoclinal folds are preserved within the dominant S1 fabric, suggesting a more complex, composite, nature to this apparent simple cleavage (Figure 5d). Thin section
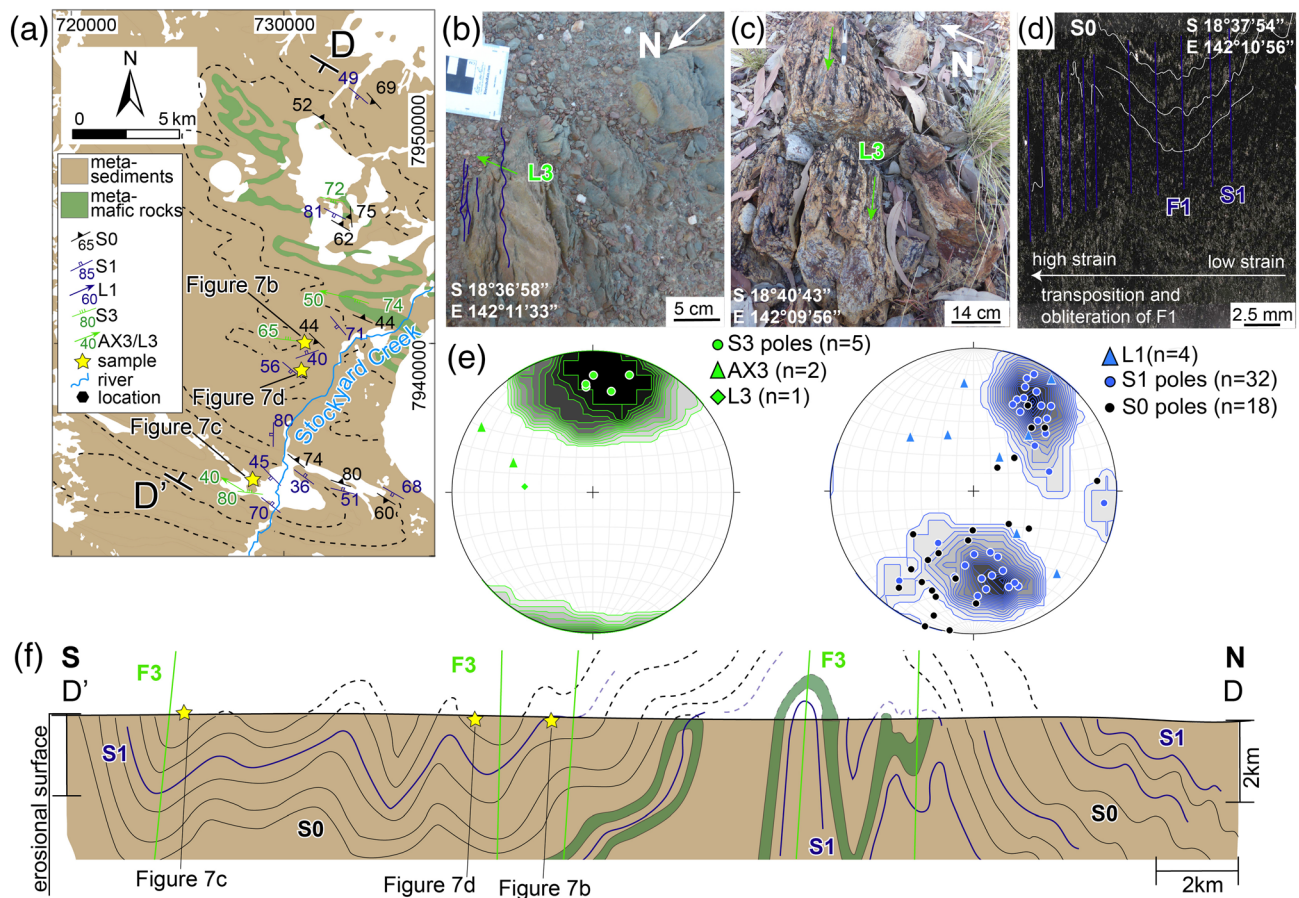
Figure 7. (a) Geological map of the Stockyard Creek area with representative structural measurements. (b, c) Field photographs showing the dominant cleavage (S1) crenulated during D3. (d) Microphotograph (plane-polarized light) of black shales preserving F1 microfolds, progressively transposed and obliterated along an F3 limb. (e) Stereographic diagrams (equal area, lower hemisphere projections) with contours of S3 poles (green) and S1 poles (blue). Corresponding linear structures are also plotted (e.g., L1, L3, and AX3). (f) Interpretative N-S geological cross section (DD′) of the dominant structures in the Stockyard Creek area.

analysis confirms that S1 has an anastomosing fabric at this location, with an earlier foliation preserved at a high angle within rare D1 low strain domains. Consequently, we consider S1 as a composite fabric, but the complexities are sporadically developed, and the continuity of S1 from Western Creek southward suggests that the pervasive S1 low-grade cleavage is the dominant fabric at the regional scale. Locally, S1 is statically overgrown by randomly oriented centimeter-scale andalusite porphyroblasts, which are generally localized in the most micaceous layers. Hence, andalusite is postkinematic to S1, but it is not accompanied by the development of a new fabric (i.e., M2a in Volante et al., 2020) in the western domain.

D3 structures. Open to tight shallowly (10–42°) W plunging and WNW trending F3 folds are commonly associated with the development of a retrograde, steep (65–88°) axial planar cleavage (S3), also defined by greenschist facies mineral assemblages (i.e., M3 in Volante et al., 2020). Strain partitioning during the D3 phase is reflected by the development of open, shallow, W plunging (15–40°), WNW- trending F3 crenulation or the development of a weak, WNW trending, steep axial planar slaty cleavage (S3; Figure 5f) in the northern area (e.g., *Western Creek*). The S3 cleavage becomes progressively more pervasive and penetrative southward (e.g., *Townley Station*). From *Flat Creek* southward (Figure 5a), F3 folds reorient earlier folds and fabrics, into a regional WNW trend which defines kilometer-scale alternations of synformal and antiformal F3 structures. Across the southernmost F3 synform in this area, S1 dip becomes progressively shallower (Figures 5f and 5g). Where steep, S1 is virtually indistinguishable from S3 and the original NNE–SSW trend of S1 and S0 is preserved only within rare F3 fold hinges.
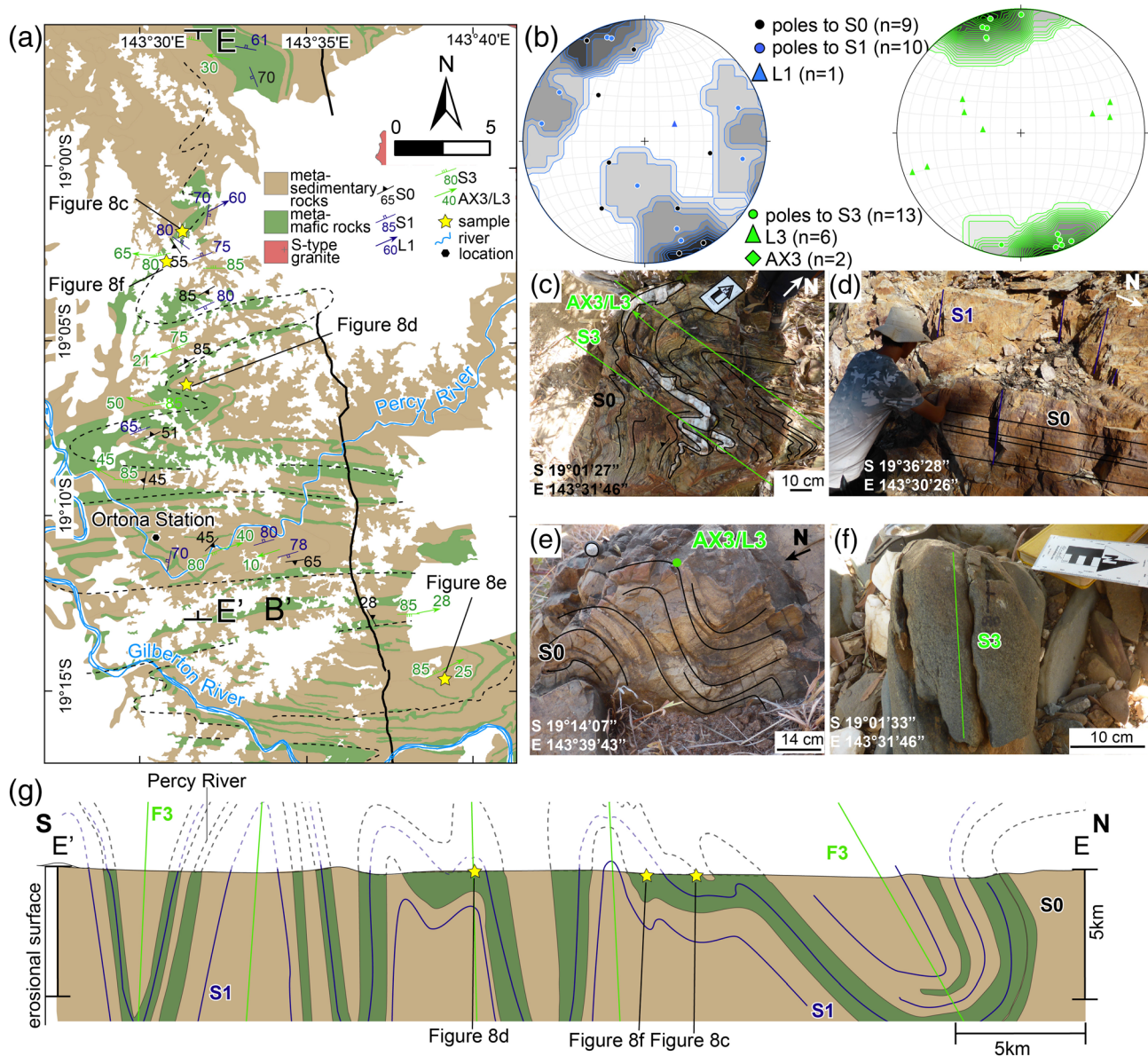
Figure 8. (a) Geological map of the Ortona Station area with representative structural measurements. (b) Stereographic diagrams (equal area, lower hemisphere projections) with the contour of the dominant cleavage S1 (blue) and the retrograde S3 cleavage (green). Poles to the bedding (S0) overlain with the S1 contour. Linear structures associated with S1 (e.g., L1) and S3 (e.g., AX3 and L3) are also plotted. (c–f) Field photographs presenting the relationships between the bedding (S0), the dominant cleavage (S1), and the retrograde S3 foliation. (g) Interpretative N-S geological cross section (EE′) of the dominant structures in the Ortona Station area.

Area 2: *Paddys Station-Western domain* (Figures 6a–6f). At this locality D1 and D3 structures were mapped.

D1 structures. In the westernmost part of this domain, around *Paddys Station* (Figure 6a), metasedimentary rocks (Figures 6b–6d) are capped in the west by flat-lying rhyolites of the Croydon Volcanics, which are nonfoliated (Figure 6e). Felsic, megacrystic granitoids locally intruded the volcanic rocks. Within the metasedimentary rocks, the bedding (S0) is preserved as alternations of pelitic and minor psammitic to beds. These metasedimentary rocks are commonly laminated slates, with the lamination defined by variations of red and gray layers (Figure 6b). In this area, NNE-SSW trending F1 folds are not observed in the field, although the stereographic projection shows a generally NNW plunging L1 lineation (Figure 6). The axial planar fabric S1 is preserved as a pervasive fine-grained foliation (locally as cleavage) either subparallel to or at moderate angles to bedding (Figures 6c and 6d). S1 is a well-developed slaty cleavage defined by very

fine-grained aggregates of muscovite–quartz–feldspar–opaque in phyllites and by elongated lozenge-shaped whitish aggregates, within a very fine-grained matrix in slates. Stereographic projections of S0 and S1, in both northern and southern segments of the cross section (CC′ in Figure 6f), show the overlapping distribution and confirm field relationships suggesting that they are subparallel (Figure 6f).

D3 structures. S1 and S0 are folded by kilometer-scale F3 folds, which vary progressively from WNW to W trending southward. In the northern area, F3 folds are open to tight, plunging moderately to shallowly (20–45°) to the WNW. Cluster distributions of poles to S0 and S1 (Figure 6f) confirm that these two fabrics were folded together by a dominant D3 deformation event. Stereographic diagrams highlight the regional variation of the F3 trend across the N-S profile. In the northern segment of the cross section (Figure 6f) F3 folds are characterized by moderately (50–70°) dipping limbs and by the development of a weak subvertical axial planar cleavage (S3). In the southern area, F3 become progressively tighter and E-W trending, where the axial planar fabric S3 is more intensely developed (Figures 6a and 6f). In this southern area, S0/S3 intersection lineations also plunge shallowly to the west, parallel to F3 fold hinges.

Area 3: *Stockyard Creek-Western domain* (Figures 7a–7f). About 15 to 20 km east of Paddys Station, at the Stockyard Creek locality (Figure 7a), a N-S profile (Figure 7f) records structural relationships between D1 and D3 structures.

D1 structures. In the northern part of this area, an antiformal D3 structure exposes the rocks of the lower part of the Etheridge Group, which conformably underlies the upper Etheridge metasedimentary rocks (Withnall, 1996; Withnall et al., 1988). Within the latter, bedding (S0) is defined by alternations of pelites and minor fine-grained psammites. Within the F3 antiform (Figures 7a and 7f), S0 is characterized by variations of pelitic and psammitic layers along with subparallel greenish-gray amphibolitic layers. Amphibolite layers define F1 isoclinal folds, while the axial planar fabric S1 is commonly subparallel to S0 (Figure 7e). In thin section, F1 microfolds are locally preserved, where the S0 is intensely folded and progressively transposed parallel to the axial planar fabric S1 (Figure 7d). S1 is a pervasive foliation, defined mainly by aligned aggregates of quartz–biotite–muscovite in phyllitic to schistose metasedimentary rocks, and by green amphibole–epidote–albite–titanite in the amphibolitic rocks. Stereographic projections (Figure 7e) show that poles to S0 and S1 from two overlapping clusters with mean orientations around 035°/30° and 170°/45°. They form a girdle with average beta (β) value (~290°) close to the measured L3 lineation, indicating refolding by the new WNW trending F3 folds (Figure 7e). Rarely, F3 hinges preserve the original N-S trend of the steep S1 foliation.

D3 structures. The second folding event in this area developed kilometer-scale, shallowly to moderately (10–50°) WNW plunging F3 folds (Figure 7e). These structures are commonly associated with the development of a steep retrograde, WNW-striking axial planar cleavage (S3). F3 folds can be traced continuously into the Paddys Station area further west. The similar geometrical distribution and orientations of the mapped structural elements in the Stockyard Creek and Paddy's Station locations highlight the consistency of the regional F3 structures across these two areas.

Area 4: *Ortona Station-Western domain* (Figures 8a–8g). The southernmost part of the study region is most intensely deformed by D3 structures, although relicts of earlier structures can be identified.

D1 structures. Bedding (S0) is defined by alternations of pelitic and more quartzitic layers interlayered with metabasalts. This sequence is cut by metadoleritic dykes. S0 is commonly subparallel to a pervasive cleavage (Figures 8a and 8b) identified as S1. Poles to the S0 and S1 form two sets with a dominant NNW-SSE and a minor WNW-ESE trend (Figure 8b). The dominant S1 foliation is locally defined by very fine-grained muscovite–quartz-bearing assemblage in the metapelites and by green amphibole–anorthite–titanite–quartz in the amphibolitic rocks. S1 is rarely preserved as a steep (65–80°) N-S trending fabric within WNW trending F3 fold hinges (Figures 8b and 8d).

D3 structures. S1 and S0 are intensely folded by regional open to tight, W trending F3 folds, which are shallow to moderately (10–60°) doubly plunging (Figure 8b). A pervasive retrograde, steep fabric is sporadically developed as axial planar cleavage (S3) of the W striking folds (Figures 8b–8g). In this area, the distinction between S1 and S3 in both metasedimentary and amphibolitic rocks (Figure 8f) is locally obliterated by the retrograde metamorphic overprint of the fine-grained mineral assemblages associated with the D3 overprint.
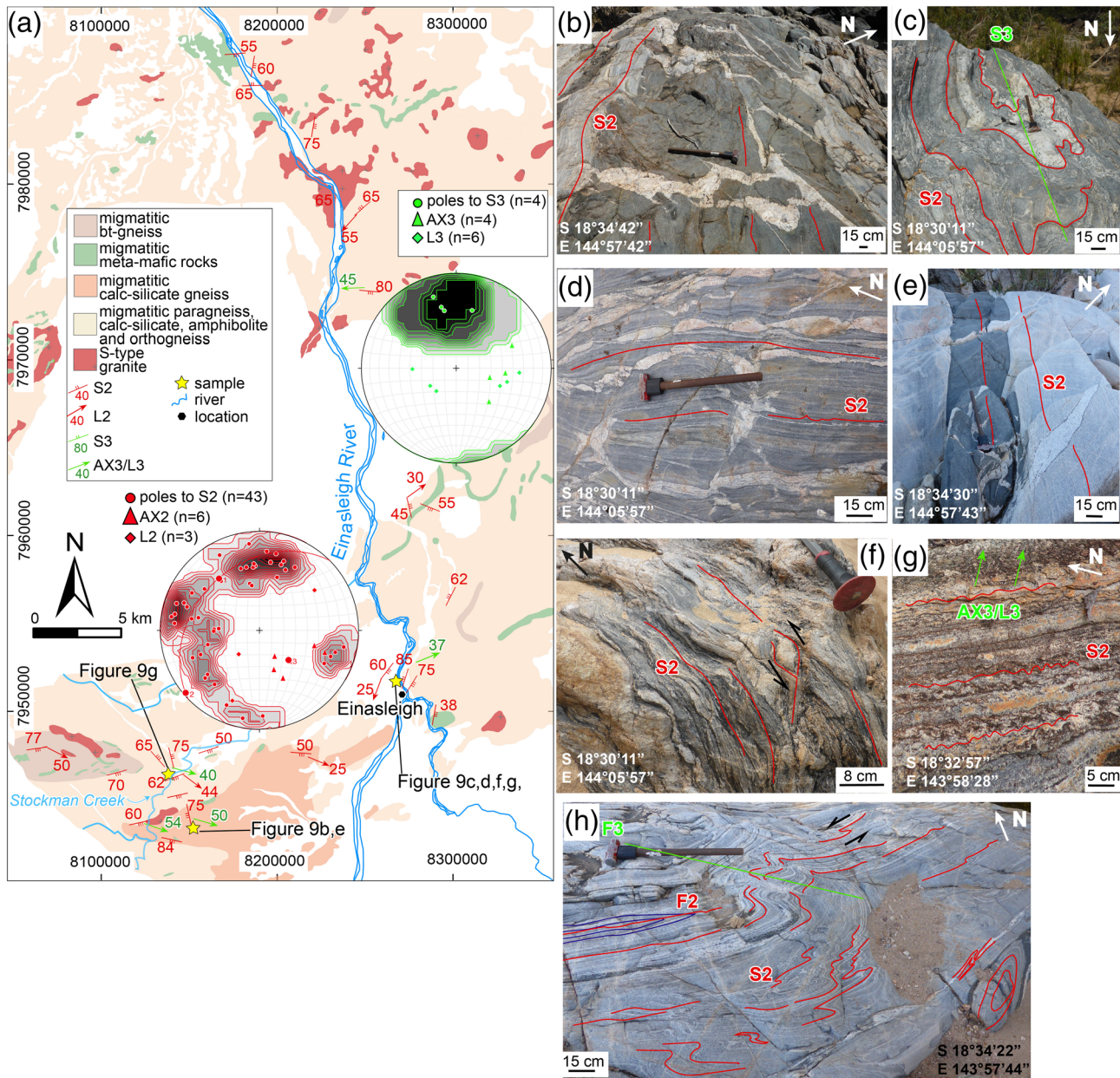
Figure 9. (a) Geological map of the high-grade eastern domain with representative structural measurements and associated stereographic diagrams (equal area, lower hemisphere projections), as density plots of poles to the dominant HT foliation S2 and the retrograde overprint (S3) with the associated linear structures (e.g., L3 and AX3). (b–g) Field photographs presenting the dominant extensional structures associated with the high-temperature D2 deformation event. (b) The dominant HT fabric (S2) is subparallel to the compositional layering defined by amphibolite and paragneiss layers. Network of leucocratic melt veins fractured the amphibolite resulting in an incoherent diatexite (Sawyer, 2008), Stockman Creek. (c) F3 open folds of the S2 foliation in paragneiss, calc-silicate, and leucocratic melt layers at Einasleigh Junction. (d) Syn-S2 extensional structures, such as foliation boudinage and boudinage of syn-S2 leucocratic layers, Einasleigh Junction. (e) S2 fabric in amphibolite and orthogneiss crosscut by post-S3 leucocratic veins, Stockman Creek. (f) S-C structures along the S2 plane, Einasleigh Junction. (g) Migmatitic S2 foliation crenulated during D3, Stockman Creek. (h) Migmatitic foliation S2 and associated isoclinal F2 folds, folding an older differentiated fabric. S2 is folded by open F3 folds, Stockman Creek.

4.3. Eastern Domain

Area 5: *Einasleigh-Eastern domain* (Figures 9a–9h). In contrast to the low-grade western domain, the eastern domain has undergone high-grade metamorphism (M2) and is characterized by extensively migmatized paragneiss, orthogneiss, amphibolite, and calc-silicate rocks (Figures 9a and 9b). In this domain, the intensity of deformation, coupled with synchronous partial melting, resulted in

sequential generations of highly ductile, complex deformation structures expressed as composite fabrics, recumbent, and refolded isoclinal folds in migmatitic layering. Lithostratigraphic boundaries were strongly transposed parallel to the migmatitic layering during the M2/D2 event at circa 1550 Ma (see section 4.1).

D2 structures. A dominant compositional layering is defined by alternations of paragneiss, amphibolite, calc-silicate rocks, and minor orthogneiss. The compositional layering is parallel to a pervasive high-grade foliation, designated as a composite S2. This fabric is a migmatitic foliation defined by (1) alternations of biotite–sillimanite-bearing melanosomes and quartz–plagioclase–K-feldspar–garnet-bearing leucosomes in paragneisses; (2) by shape- and lattice-preferred orientations (SPO and LPO, respectively) of brown hornblende and SPO of plagioclase–quartz and minor garnet interlayered with plagioclase–quartz–garnet-bearing leucocratic veins in amphibolitic rocks; (3) by amphibole–titanite–epidote–garnet and minor quartz–plagioclase–biotite in the calc-silicate rocks, and (4) by amphibole–titanite–feldspar–quartz assemblage in the orthogneisses. Therefore, S2 is a composite high-grade axial planar fabric of F2 refolded, recumbent tight to isoclinal folds (Figures 9b–9h) defined by an older differentiated foliation, which is commonly obliterated during migmatization (Figure 9h).

Stereographic projections of the S2 poles (red in Figure 9a) show a girdle distribution with two well-defined clusters at 290°/25° and 000°/30°, reflecting the dominance of moderately to more rarely steeply (40–75°) E and S dipping S2 in the area. Nonetheless, a N-S orientation of the plane of the dominant migmatitic fabric S2 is locally preserved within F3 hinges. The poles to S2 show that this foliation is overprinted by approximately NW-SE to E-W trending F3 folds (Figure 9a). Unfolding the dominant E-W trending F3 folds within this region indicates that the folded, S2 surface was originally N-S striking, which coincides with S2 enveloping surface. Additionally, a shallow to moderate (25–45°) dominantly SE plunging, with rare NW and SSW plunging, L2 mineral lineation, defined by aligned sillimanite and biotite, is locally preserved. F2 hinges and mineral lineations (L2) form a scattered SW-NE girdle distribution indicating that F2 folds are noncylindrical and have been refolded likely during the D3 deformation overprint (Figure 9a). Mesoscopic F2 disharmonic folds or F2/F3 interference pattern occur in the hinge of a macroscopic F3 fold in the Stockman Creek locality (Figure 9h) and were previously interpreted as F2 sheath folds by Hills (2003). These complex fold structures are common in the Einasleigh, especially in calc-silicate and biotite-gneiss, adjacent to the lithological boundary of these rock types described by Hills (2003) in the Stockman Creek location. F2 hinges are commonly moderately to steeply SE plunging (Figure 9a and 9h). Both symmetrical (e.g., foliation boudinage or boudinage of leucocratic layers; Figure 9d) and asymmetrical (e.g., pressure shadows of leucocratic material around garnet crystals or S–C′ structures; Figures 9f and 9h) extensional structures developed parallel to the dominant migmatitic S2 fabric and suggest a sinistral (top to the left) shear sense.

Leucocratic segregations are commonly observed in boudin necks, subparallel to S2 and along local shear zones of the asymmetrical foliation boudinage, indicating that melt was present during the development of S2. Melt segregations have two different grain sizes: fine-grained quartz–feldspar-rich leucocratic layers are commonly subparallel to the dominant migmatitic foliation, whereas coarse-grained to pegmatitic muscovite–biotite–quartz–feldspar veins developed both subparallel and oblique S2, commonly forming a chaotic network of veins (Figures 9b, 9d, and 9e). The described field relationships between D2 structures and leucosomes indicate that the principal extension direction lies close to the plane of the migmatitic foliation and that melt segregation also occurred syn-, late-, to post-S2.

D3 structures. Mesoscopic F3 folds are the most common folds observed in this subarea. The migmatitic foliation S2 is reorientated into macroscopic F3 upright, steeply dipping, E-W trending, doubly plunging folds, which vary from shallow to moderate plunging (25–55°) to the west and east (Figures 9a and 9c). F2 folds are refolded during D3, producing local high amplitude interference folds. Moreover, S2 outlines an open E-W trending F3 crenulation pattern, associated with a consistent E-SE plunging crenulation lineation (L3; Figures 9a and 9g). The slight variability in F3 plunge could be the result of later N-S trending folding (F4), as previously suggested (e.g., Withnall, 1996). Locally, a retrograde, steep crenulation cleavage developed axial planar to E-W microfolds (S3). Leucosomes were rarely observed in F3 hinges but not in the S3 axial planar fabric (Figure 9c). In the southern part of the Einasleigh area, along the northern limb of the regional F3 fold, the intense retrogression of mineral assemblages along the axial planar fabric within

paragneiss, calc-silicate, and amphibolite was previously interpreted as a major shear zone at the contact between biotite-bearing gneiss and calc-silicate (Hills, 2003). One kilometer south of this shear zone, local tension gashes filled with quartz–feldspar-bearing melt (Figure 9e) crosscut the S2 migmatitic foliation and were previously dated using U-Pb geochronology on zircon, at circa 1545 Ma (Hills, 2003). This age places a minimum constraint on D3 deformation in this region.

4.4. Central Domain

Between the western greenschist and the eastern upper-amphibolite facies domains lies the central domain, where middle- to upper-amphibolite facies conditions were recorded. In this domain, D1–D3 structures were identified.

Area 6: *Lornevale Station-Central domain* (Figures 10a–10h).

D1 structures. Between Forsayth and Georgetown (Figure 3), at the *Lornevale Station locality* (Figure 10a), amphibolitic layers define upright, tight kilometer-scale, NNE-SSW trending F1 folds, concordant to the F1 folds observed in the adjacent Western Creek area. The axial surface of these folds is recorded in fine-grained schists as a steep (65–85°), SE dipping pervasive S1 foliation, marked by white mica–quartz–biotite. However, further eastward, these F1 folds are truncated and obliterated by the development of a shallow, W dipping, N-S striking S2 fabric (Figures 10a and 10b). In most of Area 6, S2 dips steeply with an E-W to NE-SW strike caused by F3 folding (Figure 10b).

D2 structures. The transition from D1 to the D2 structural overprint is best observed on a road section ~20 km south of Georgetown (Figure 8a). At this location, highly foliated schists (e.g., sample RR52; Figure 8c) preserve a shallow (~30°) west dipping schistosity (S2) defined by major white mica and minor biotite–garnet–andalusite.

Microstructural analysis of the schists reveals relicts of an older fabric within low strain domains of the shallow overprinting S2 foliation. This relict fabric (S1) is defined by white mica–biotite–quartz. In this transition zone, S2 is a differentiated fabric characterized by alternations of mica-rich layers (M domains), composed of dominant white mica alignment and minor biotite–opaque (oxides?), and quartz-rich layers (Q domains), characterized by quartz and the relict S1 fabric. Locally, round to hexagonal shaped aggregates of oxides(?)–plagioclase–epidote–biotite are wrapped by the dominant S2 foliation and likely represent garnet relicts. The development of D2 structures is most evident as an obvious reorientation of the NE striking, SE dipping, low-grade S1 fabric, to a N striking, W dipping higher-grade S2 foliation.

East of *Lornevale Station*, within the D2 zone (Figure 10a), schistose metasedimentary rocks become progressively more gneissic spatially, associated with an increase in abundance of granitic intrusions (Figure 10d) and extent of migmatization of the hosting metasedimentary rocks (Figures 10e–10g). In this area, the dominant shallow, high-grade foliation S2 is a complex gneissic axial planar fabric of inclined to recumbent isoclinal folds (F2). An ESE plunging mineral lineation (L2), commonly defined by biotite or sillimanite in metasedimentary rocks and hornblende in amphibolite, is subparallel to rare F2 fold hinges (AX2) (Figure 10b). In migmatitic paragneisses, S2 is defined by restitic biotite–sillimanite-bearing M domains interlayered with leucocratic (quartz–plagioclase–K-feldspar–garnet-bearing) layers. In amphibolitic and granitic rocks, S2 is marked by brown amphibole–plagioclase–quartz and by elongated partially recrystallized K-feldspar wrapped by biotite–plagioclase–quartz–muscovite-bearing matrix, respectively (Figure 10d). The S2 composite fabric and associated leucocratic layers are intrafolial and axial planar to centimeter to kilometer and regional scale, reclined to recumbent F2 folds. The progressive development of the complex S2 fabric occurred under partial melting conditions and continuous melt segregation. The progressive deformation during D2 is characterized by intense folding (F2) of a high-grade differentiated, composite S2 fabric (Figures 10e and 10f). With increasing strain, these F2 folds are tighter and display a strong axial planar differentiated foliation, likely an evolved stage of S2 (Figure 10f). In D2 high strain zones, F2 folds are progressively pinched and transposed by the development of an intense and penetrative axial planar fabric (evolved S2), which progressively obliterated the early F2 hinges and transposed the F2 limbs parallel to S2 (Figure 10g). Similarly, to the eastern domain, a slight scatter of L2 and AX2 from E to SW might reflect the structural complexities associated with the D2 deformation event and/or to a subsequent folding event (possibly both F3 and F4; Figure 10b).
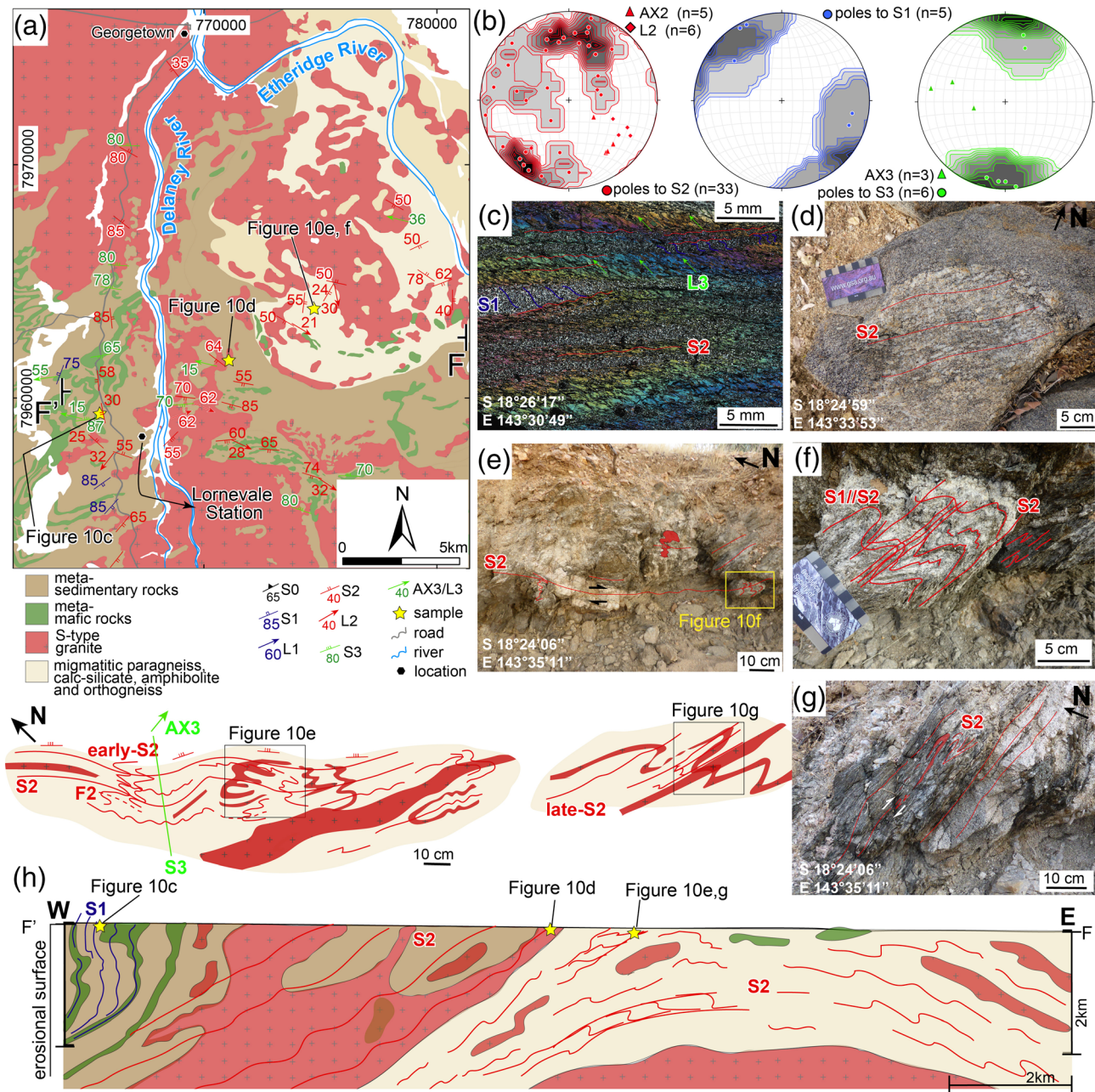
Figure 10. (a) Geological map of the Lornevale Station area with representative structural measurements. (b) Stereographic diagrams (equal area, lower hemisphere projections) with contours of the dominant HT foliation S2 and the associated lineation (L2), the older fabric/s (S1) and the younger overprint (S3) with the related lineation (e.g., L3 and AX3). (c) Microphotograph of a phyllitic schist (i.e., sample RR52) preserving the oldest S1 fabric within S2 low strain domains. S2 in crenulated by the D3 event. (d) Photograph of the Delaney granite deformed during the D2 deformation event and recording a pervasive S2 fabric. (e) Photograph and interpretative sketches of partially melted paragneisses, where the composite fabric S2 is an intrafolial axial planar fabric of recumbent isoclinal F2 folds. Leucocratic layers were folded during early-S2 development and are subparallel to the F2 limbs, during the late stages of S2 development. F2 are gently refolded by east plunging open E-W striking F3 folds. (f) Close up of Figure 10e. (g) D2 shear zone where F2 folds are transposed parallel to the pervasive axial planar composite fabric S2. (h) W-E cross section (FF′) from the Western Creek low-grade area to the eastern higher grade and partially melted metasedimentary rocks intruded by voluminous granite sheets.

At the regional-scale, these observations indicate that the shallow W dipping S2 foliation progressively obliterated older S1 fabrics eastward and become the pervasive composite gneissic foliation in the central domain. Moreover, medium to coarse-grained leucocratic layers are commonly subparallel to more restitic

biotite–sillimanite-rich layers defining the dominant S2 gneissic fabric in the metapelite. Field observations confirm that S2 developed syn- to late/postemplacement of granitic leucosomes.

D3 structures. D2 structures are folded by open, W-plunging F3 folds (Figures 10b, 10c, 10e, and 10h) developing a crenulation at the mesoscale and microscale. Brown biotite is commonly aligned parallel to the crenulation hinges (Figure 10c), while locally a weak retrograde subvertical axial planar foliation (S3) developed in F3 fold hinges.

Area 7: *Robinhood Station-Central domain* (Figures 11a–11k**)**. *At the Robertson River locality*, *between Cobbold Gorge and Robinhood Station* (Figure 11a), two W-E transects (Figures 11a and 11b) show the transition of the mapped fabrics from the low-grade western domain to the higher-grade fabrics of the central domain.

D1 structures. In the westernmost segment of the GG′ cross section (Figure 11b) bedding (S0) in fine-grained phyllite is marked by alternations of laminated pelitic and more psammitic layers (Figure 11c). A pervasive S1 cleavage is oblique to S0 and is defined by oriented porphyroblasts of biotite, aggregates of fine-grained white mica, and minor fine-grained quartz–opaque aggregates, ascribed as S1 (Figure 11d). Biotite is commonly replaced by a very fine-grained assemblage of white mica and quartz. Rarely, in E-W trending F3 fold hinges, S1 is preserved with its original N-S orientation (Figure 11a). In this western part of the cross section (i.e., Cobbold Gorge and Malcolm Creek areas; Figure 11a), S1 is commonly associated with a mineral lineation (L1) defined by the preferred orientation of orange to brown biotite, which is typically plunging shallowly (~30°) to the NNE.

Farther to the NE of the *Cobbold Gorge locality* and northwest of the *Robinhood Station* (Figure 11a), S0 is defined by amphibolite within dominant schists and minor calc-silicate and quartzite. In this region, during the 1600 Ma D1 event, a composite fabric S1 is developed. Different stages of S1 development (Bell & Rubenach, 1983) were recorded at Cobbold Gorge (RR29 in Volante et al., 2020) or in the hinge of F3 folds (Figure 11e). S1 is defined by muscovite, biotite, elongated, flattened quartz, medium to large (1–5 mm) euhedral to subhedral poikilitic staurolite, and euhedral to subhedral garnet porphyroblasts. At the microscale, S1 is a composite fabric where S1a occurs as ilmenite and quartz inclusion trails in staurolite and garnet subhedral porphyroblasts set within Q domains of the S1b foliation (Figures 11f and 11g). In both garnet and staurolite, S1a relicts are at a high angle (in the center of the grains; grt_a for garnet) to curvilinear inclusion trails (toward the edge of the grains; grt_b for garnet) that are subparallel and continuous with the external foliation S1b (Figure 4). Both garnet and staurolite feature quartz-rich pressure shadows with minor biotite. Within the mica-rich layers defining the dominant differentiated fabric, staurolite grains and minor garnet rims (grt_b) are subparallel. We ascribe this staurolite–garnet fabric as a progressive foliation S1, preserved within the quartz-rich domains during early stages of its development (S1a) and by the matrix foliation during the later stages of differentiation (S1b). Hence, grt_a grew early-S1 (S1a), while grt_b and staurolite are syn- to late-S1 (S1b). These microstructural observations were confirmed by the contrasting chemical composition of grt_a and grt_b (Volante et al., 2020). In the field, S1b is moderately (30–55°) to steeply dipping (60–80°) along limbs and hinges of E-W kilometer-scale F3 folds, respectively (Figure 11a). Structural measurements of the composite fabric S1 are comparable with a foliation identified as S1/2 and associated with a FIA3 (N-S) by Cihan and Parsons (2005). S1b is commonly associated with a NNW plunging biotite mineral lineation (L1) in the *Robertson River* and *Cobbold Gorge* localities. The bimodal orientations showed by L1 in the Robinhood Station subarea might reflect two sets of D1 structures associated with the 1600 Ma S1 composite planar fabrics (i.e., S1a and S1b) or might represent the effect of the subsequent deformation event D2, which also developed dominant N-S striking structures but is associated with E-W extension. In either case, the variation of the F1/L1 structural fabrics is consistent with previous structural data obtained in the same area and associated with a composite fabric ascribed as S1/2 (Cihan & Parsons, 2005).

D2 structures. The amount of granitic material increases eastward as the metamorphic grade reached medium- to upper-amphibolite facies. Accordingly, the older staurolite–garnet-defining foliation (e.g., S1a and S1b) is progressively overprinted by a subparallel andalusite/sillimanite–biotite–white mica–quartz–plagioclase–ilmenite composite fabric (S2) developed (Figure 4). This S2 fabric is shallow to moderate (20–50°) W dipping and is axial planar of recumbent isoclinal folds (F2; Figures 11j and 11k), where the dominant compositional layering S0 is subconcordant to S1 and S2. F2 folds are characterized by moderate (20–50°),
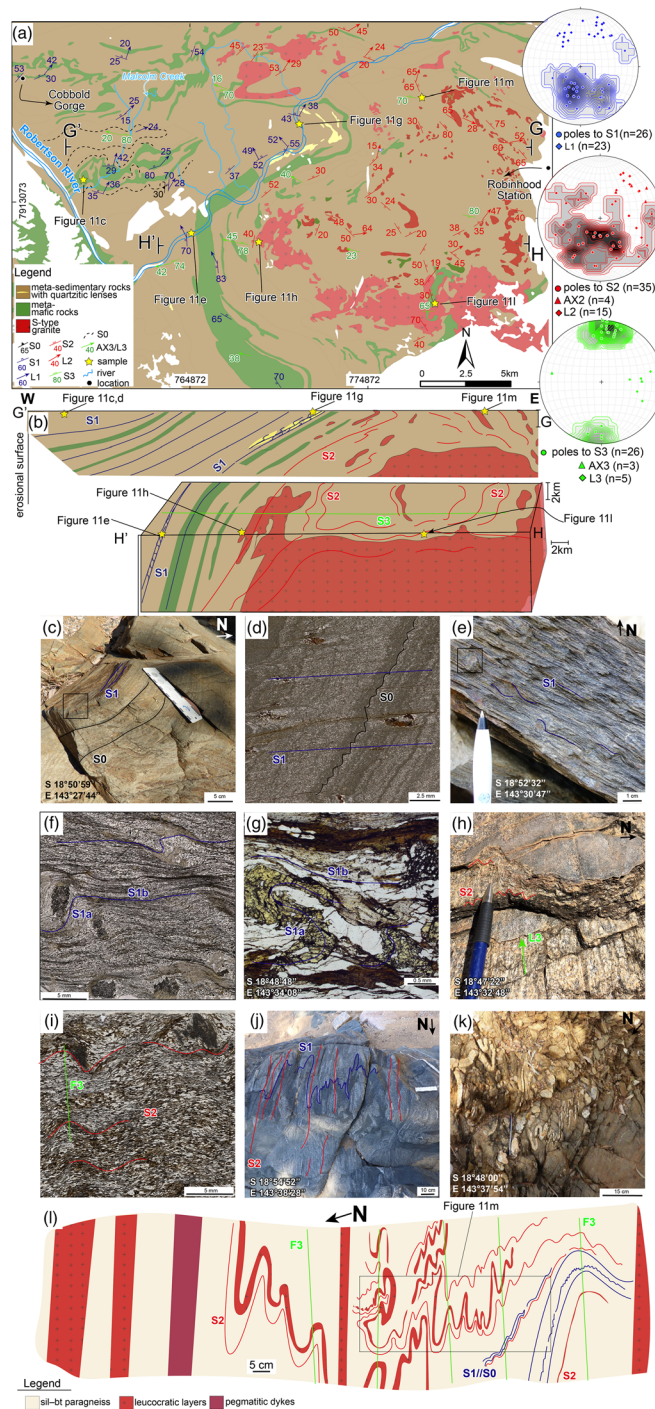
Figure 11. (a) Geological map of the Robinhood Station area with representative structural measurements and stereographic diagrams (equal area, lower hemisphere projections) with contours of the poles to the dominant HT foliation S2, the poles to the composite S1 fabric/s and the poles to S3. Lineation (Ln) and fold axis (AXn) associated with each fabric generation are also plotted (i.e., L1, L2, AX2, L3, and AX3). (b) W-E cross sections (GG′ and HH′) from the low-grade western area to the eastern higher grade and granite-bearing area. (c, d) Field- and microphotographs, respectively, of the relationships between the bedding (S0) and the phyllitic axial planar cleavage (S1) in an F3 hinge. (e, f) Field- and microphotograph, respectively, of the composite fabric S1 in garnet-bearing schist. (g) Microphotograph of the composite fabric S1 in staurolite-garnet-bearing schist. (h, i) Field- and microphotographs of the shallow composite sillimanite-biotite-defined S2 foliation, crenulated during the D3 deformation event. (j) Tight to isoclinal F2 folds in amphibolite recording incipient melting subparallel to the axial planar fabric S2. (k) Open to tight F3 folds of paragneiss and leucocratic layers refolding isoclinal F2 folds. (l) Representative sketch of the outcrop in Figure 11k.

NE and E plunging fold hinges (AX2) and a local mineral lineation (L2) defined by andalusite or sillimanite (Figure 11a). The scatter shown by L2 likely reflects the composite nature of the complex D2 structural elements (e.g., S2a and S2b) or might be explained by the overprinting F3 folding event. In this case, no structural features associated with the described high-grade sillimanite-bearing fabric were identified by Cihan and Parsons (2005). In contrast, these authors interpreted the successive deformation event to be associated with FIA4 (NE-SW) and the development of a NE-SW striking S3/4 fabric and a NE-trending linear fabric within the staurolite stability field. These observations disagree with our study that identified, instead, an extensional, N-S striking, composite S2 fabric associated with NE-E trending L2 as the regional high-temperature deformation event overprinting D1 structures and M1 mineral assemblages.

Fold asymmetry, leucocratic pods and/or pressure shadows of leucocratic material around rigid porphyroblasts as well as the regional E-plunging L2 lineation suggest a regional sinistral (top to the left) shear sense during partial melting along the S2 foliation surface.

Moreover, the association of recumbent isoclinal F2 folds with the development of a shallow sillimanite-bearing axial planar fabric S2, typically related to subparallel granitic sheets and leucocratic layers, suggests that the D2 structures are extensional. In this area as in the eastern domain, type 2 and 3 interference patterns, defined by coarse-grained leucocratic syn-S2 layers, are preserved sporadically in sillimanite-bearing schists (Figures 11k and 11l). Locally, pegmatites are oriented parallel to the F3 orientation (Figure 11l), and the leucocratic interlayered material is also foliated subparallel to S2. Therefore, S2 developed syn-, late-, to postmigmatization and granite emplacement. Extensional markers along the S2 plane, such as boudins of the leucocratic layers, S-C structures, pinch-and-swell structures and the plunges of D2 linear fabrics indicate an ENE-WSW transtensional movement of the regional W-dipping S2 plane (Figure 11a).

D3 structures. During this deformation event, S0, S1, and S2 were refolded (Figures 11k and 11l) into kilometer to microscale open to tight E-W trending, shallowly (15–40°) E-W doubly plunging folds (F3). The variation in the orientation of the F3 plunges might reflect a younger N-S trending folding event that also further reorientation of F2 plunges. F3 folds are commonly associated with a steep, retrograde axial planar cleavage S3 (Figures 11h, 11i, and 11l). Locally, in the easternmost part of the central domain, pegmatitic dykes are oriented parallel to the F3 axial planar fabric, suggesting that residual granitic melts persisted during this younger D3 deformation event (Figure 11l).

The interference patterns between F3 and F2 folds are commonly observed at the macroscale across the inlier but are rarely preserved at the mesoscale (Figure 3). The two generations of folds developed mushroom-type interference pattern (Ramsay, 1967) that reflects approximately coaxial refolding of F2 recumbent isoclinal folds by upright tight to open F3 folds (Figures 11k and 11l).

5. Discussion

The following discussion is divided into five sections. In the first section (5.1), the deformation history is summarized and correlated across the inlier based on our petrographic and structural study and in association with recently published microstructural, geochronological, and petrological results (Volante et al., 2020). Section 5.2 focuses on the progressive versus episodic deformation concept and how this is applied to our study area. Section 5.3 emphasizes the approach used in this paper to unravel the structural evolution of the region with an evaluation of the previously applied FIAs technique. Sections 5.4 and 5.5 put this petrographic and structural multiscale study into the context of the supercontinent Nuna.

5.1. Structural Evolution of the 1.60–1.50 Ga Orogenic Event in the GTI
5.1.1. First Deformation Event (D1)
D1 structures (e.g., S1a and S1b) in the western and central domains were identified microstructurally and dated using Lu-Hf in garnet and U-Pb in monazite geochronology at circa 1600 Ma (Volante et al., 2020). Regional mapping of the Western Creek area has identified the original orientation of the F1 folds and the associated S1 fabric, to be NNE trending (Figure 5). The geometry of the F1 folds as upright, slightly inclined folds and the steepness of the associated axial planar fabric S1 indicate that these structures developed under a compressive tectonic regime with a dominant WNW-ESE shortening direction (Figure 12a). The bimodal orientations of the linear fabrics associated with S1/F1 (i.e., L1/AX1) might
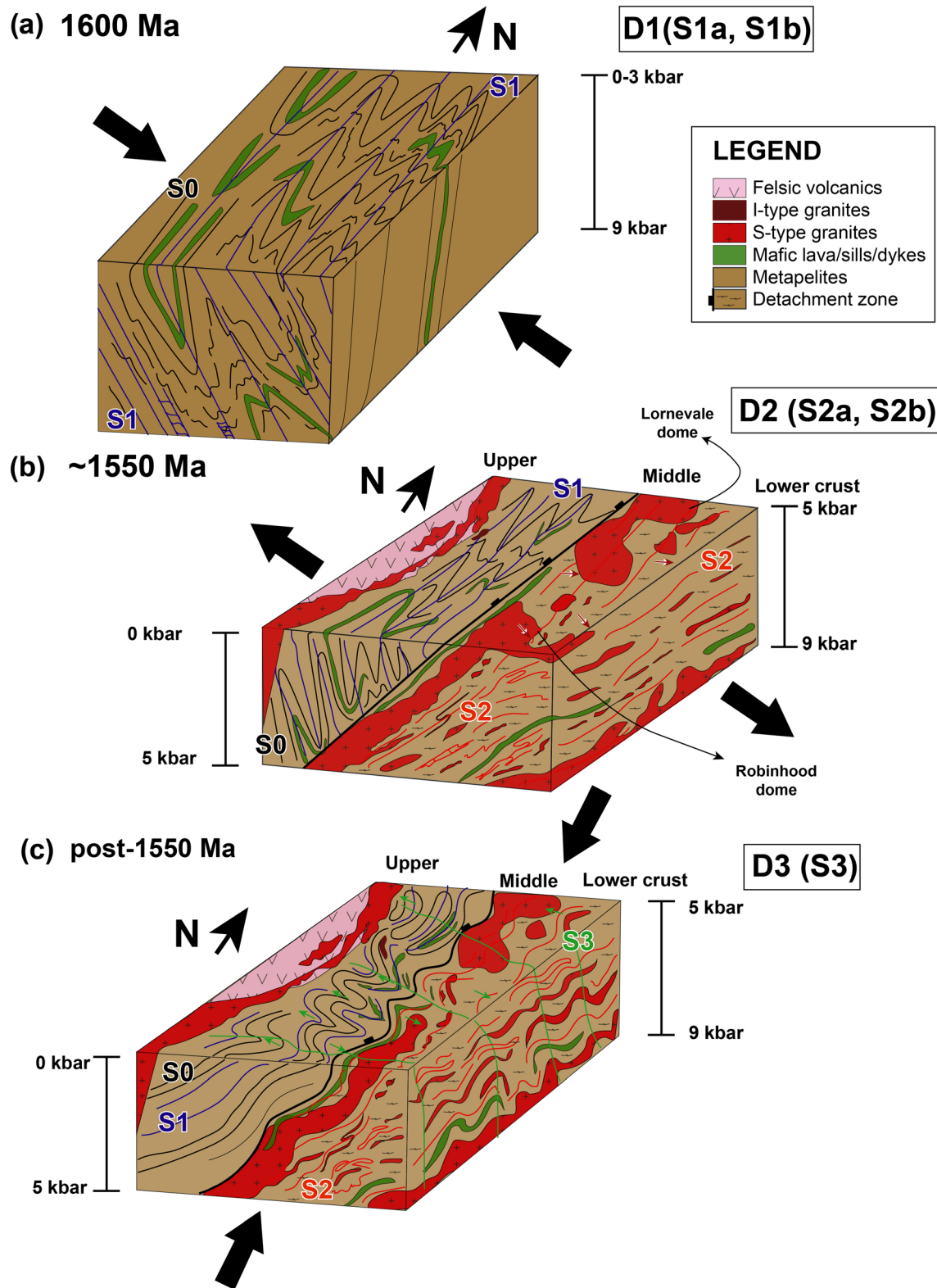
Figure 12. The 3-D interpretative structural model of the GTI illustrating the main structural relationships in the different crustal domains. (a) E-W compressional event during the D1 event at circa 1600 Ma developed N-S striking compressional composite S1 fabric (foliation trajectory in blue). (b) E-W extensional D2 event at circa 1550 Ma associated with the development of a shallow high-grade foliation surface S2, which coincides with a west dipping detachment zone. This crustal-scale shear zone is associated with the migration of localized granitic sheets through the crust. The Lornevale and Robinhood granite dome were exhumed during transtensional shear along the detachment fault. (c) Post-1550 Ma D3 phase developed E-W striking doubly plunging F3 folds.

reflect two sets of D1 linear structures. This interpretation also agrees with S1 being a composite fabric (i.e., S1a and S1b) and with previous structural work (Cihan & Parsons, 2005). D1 deformation occurred simultaneously under greenschist facies and midamphibolite facies in the western and in the central domains, respectively. Our results show that the circa 1600 Ma D1 deformation event was associated with E-W compression related to the continental collision between the GTI and the MTI (e.g., Pourteau et al., 2018)

As described in section 4.2, area 2 (Paddys Station) records a dominant S1 foliation, subparallel to S0, all within the westernmost metasedimentary rocks. However, previous researchers suggested that the uppermost part of the metasedimentary sequence in the western domain (i.e., Langlovale Group) was deposited after the first deformation event (Neumann & Kositcin, 2011; Withnall & Henderson, 2012). This interpretation was based on an inferred unconformity between the Langlovale Group and the underlying upper part of the Etheridge Group (Withnall & Mackenzie, 1980). Our mapping shows that D1 deformation fabrics are evident in all these rock types, and the unconformity is not recorded. Instead, the local low-angle discordances observed at regional-scale reflect the same early structural complexity throughout the entire inlier. Therefore, we infer that the Langlovale Group and the Etheridge Group are part of a conformable single sedimentary succession, as suggested by Nordsvan et al. (2018), based on sedimentology and detrital zircon geochronology. In the eastern migmatitic domain, evidence of D1 is rare and difficult to identify as they were pervasively transposed during D2/M2.

5.1.2. Second Deformation Event (D2)

The second deformation event is extensively recorded in the central and eastern domains but not in the western domain where static overgrowth of andalusite over S1 at circa 1550 Ma (M2a in Volante et al., 2020) also indicate that D2 did not affect the domain. This dichotomy might reflect the presence of a tectonic contact between the western and the central domains, which is pervasively overprinted by the D2/M2 event (see discussion below).

In contrast to the western domain, D2 structures and overprinting *LP–MT/HT* metamorphism are dominant in the central domain. The high-grade composite S2 foliation is locally defined by andalusite alignment (M2a) during the early stages of its development (S2a) but is predominantly characterized by sillimanite–biotite (M2b) in the later stages (S2b), where sillimanite formed as pseudomorphs after andalusite (Figure 4). The high-grade S2 fabric is a regional N-S striking, W dipping enveloping surface that truncates and overprints D1 structures and coincides with the contact between the western and the central domain. As described in sections 4.3 and 4.4 (i.e., Areas 6 and 7), structural relationships show that the complex gneissic S2 fabric developed synchronously with the intrusion of voluminous sheeted granitic bodies and extensive migmatitic leucosomes. The granites are concentrated within the central domain, where the metamorphic peak of the hosting sillimanite–biotite-bearing metasedimentary rocks is constrained at ~5 kbar and ~650°C during the D2/M2 event. Syn-D2 migmatization in the eastern domain occurred at deeper levels, at ~8 kbar and ~750°C (Volante et al., 2020).

In situ U-Pb ages, derived from monazite aligned with the S2 foliation in sillimanite–biotite-bearing metasedimentary rocks, confirm the syn-D2 circa 1550 Ma *LP/MP–HT* metamorphism and partial melting event in both central and eastern domains (Volante et al., 2020). These ages for the D2/M2 stage are comparable with magmatic zircon U-Pb ages of the felsic intrusions (Black et al., 1998, 2005; Neumann & Kositcin, 2011). The S2 gneissic foliation within the granites and migmatites is locally intensely refolded as F2 intrafolial folds, suggesting that deformation was active throughout granite emplacement and melt segregation. In both the central and eastern domains symmetric extensional foliation boudinage and boudinage of leucocratic layers indicate development under near-coaxial pure shear conditions. On the other hand, the identification of asymmetrical structures such as pressure shadows of leucocratic material around garnet crystals or S-C′ structures, along with asymmetric folds, suggest top-to-the-west shear sense along the S2 plane and provides evidence of local noncoaxial deformation (Figures 6b, 6d, and 6f). D2/M2 high-grade ductile, shear structures reflect a kilometer-thick zone of high, heterogeneous strain, as illustrated by the widespread recognition of complex fold structures in regions of intense mid-crustal deformation (e.g., Ghosh & Sengupta, 1987; Holdsworth & Roberts, 1984; Platt, 1993).

Therefore, syn-partial melting D2 extensional and shearing structures, with a regional sinistral shear indicate that the S2 surface (i) accommodated transtensional exhumation of both the Lornevale and the Robinhood granitic domes (~5 kbar) and within the underlying eastern migmatite complex (~8 kbar) and

Tectonics

(ii) coincided with a syn-extensional detachment zone. The dominant ESE-ENE-plunging L2 lineation related to the high-grade composite S2 fabric reflects the direction of transport along the crustal shear zone. A shallow W dipping crustal-scale detachment zone is consistent with the dominant W dipping structures doing down to the middle and lower crustal levels that were imaged on the deep seismic profile of the GTI (Korsch et al., 2012).

Therefore, the D2 deformation event is inferred to have developed during a post collisional E-W oriented extensional stage associated with a crustal-scale detachment zone accommodating crustal melting and exhumation of deeper crustal levels. This crustal-scale structure juxtaposed the western domain to the central and eastern domains, where upper greenschist to lower-amphibolite, and middle to upper conditions were recorded at circa 1550 Ma, respectively, and where pervasive D2 structures recorded in the central domain truncate the NNE trending F1 folds preserved in the western domain (Figure 12b). Therefore, metamorphic and structural records in the GTI suggest that the western, central, and eastern domains represent different levels of the post collisional continental crust at circa 1550 Ma and upper, middle, and lower crustal levels, respectively. The consistent top-to-the-west shearing along the high-grade S2 fabric in the central and eastern domains, suggests that crustal stretching occurring during the D2 extensional stage was accommodated by an asymmetric detachment system (e.g., SeyİToĞLu & Veysel, 2015) at circa 1550 Ma. Although this bounding zone is a W dipping plane at crustal-scale, its internal structure is characterized by complex ductile structures coupled with extensive granitic melt segregation.

5.1.3. Third Deformation Event (D3)

The youngest regional folding event (D3) is recorded as centimeter- to kilometer-scale WNW-ESE to E-W trending F3 folds that dominate the present-day regional structural pattern of the inlier. These structures are open to tight, upright shallow doubly plunging compressional F3 folds which developed a steep S3 axial planar fabric. During D3, deformation was regionally highly partitioned: D3 high-strain domains developed in pelitic-rich areas of the inlier (e.g., Area 4, Ortona Station) and along lithologic contacts (Hills, 2003). In these D3 high-strain zones, the older structures are strongly reoriented and transposed into the dominant E-W D3 orientation, where S3 often developed under low-amphibolite to upper-greenschist facies conditions (Figure 11l).

In the southern part of the eastern domain, the S2 is intensely crenulated and F2 folds are refolded by E plunging and E-W trending F3 folds, producing local open disharmonic folds or F2/F3 interference pattern. Peak M2 mineral assemblages are locally intensely retrogressed. According to field and microstructural relationships (Volante et al., 2020) and previous structural study in this area (Hills, 2003), this event occurred post-1550 Ma as it overprinted and reoriented D2 structures and replaced M2 metamorphic assemblages (Figure 12c).

Moreover, retrograde lower amphibolite facies mineral assemblages defining the S3 foliation and local, E-W trending, muscovite–quartz–feldspar–tourmaline syn-S3 pegmatitic dykes in the central and eastern domains suggest that D3 event occurred soon after peak metamorphism (post-M2) at *LP–MT/LT* metamorphic conditions. Possibly, the circa 1545 Ma leucocratic veins crosscutting the migmatitic 1550 Ma S2 foliation in the eastern domain (Hills, 2003) constrains the younger D3 event, which reflects the exhumation of the terrane under a regional N-S shortening direction.

5.2. A Combination of Progressive and Episodic Deformation

Structural analysis provides a relative chronology of superimposed generations of structures and deformation events that can be construed to be either progressive or episodic in a region. Numerous studies have previously speculated that superimposition of structural elements can occur during a single deformation event (Bell, 1978; Bell & Hobbs, 2010; Tobisch & Paterson, 1988; Williams & Zwart, 1977). The conventional approach used to distinguish between progressive and episodic deformation is the application of traditional structural overprinting criteria such as fabric reorientation, kinematics of successive structures, and strain partitioning (Holdsworth, 1990). However, structural criteria alone are not always sufficient to discriminate between progressive or discrete deformation. A crucial potential discriminant is the combination between the structure generations and their defining mineral assemblage, which could determine whether fabrics formed under similar *P–T* conditions.

In the GTI, progressive fabric development has been previously described by Bell and Rubenach (1983). Along with Reinhardt and Rubenach (1989), microstructural criteria from the central domain were used to suggest that increasing metamorphic grade was associated with six progressive stages of schistosity development, following crenulation of an older foliation. In particular, the Bell and Rubenach (1983) model describes the progressive development of a new fabric (i.e., S2) in six main stages, from open crenulation (stages 1 and 2) of an older fabric (i.e., S1) through crenulation cleavage (stages 3 and 4) to a penetrative S2 schistosity (stages 5 and 6) with no microfolds of S1 or quartz-rich microlithons remaining. During stage 3, mica- and quartz-rich microlithons are produced by rotation of S1 micas and solution transfer of quartz. In contrast, in stage 4, new mica grains in the mica-rich layers grow parallel to the axial planar fabric S2. Stage 5 shows a layer-differentiated schistosity, in which the rare mica grains of the quartz-rich layers grow parallel to the S2 axial plane. In the final stage 6, quartz from the mica-rich layers in stage 5 is inferred to dissolve and nucleate in the mica-rich layers (and vice versa), producing a uniform, penetrative S2 schistosity.

In the central domain, Bell and Rubenach (1983) suggested that all six stages of D2 were heterogeneously recorded, with porphyroblasts preserving earlier stages of S2 development relative to the matrix. In particular, they interpreted garnet to grow during the early stages of D2, followed by staurolite–biotite (stages 3 and 4) and successive andalusite–biotite (stages 4 and 5) to the stage 6, which they related to sillimanite growth. The sequence of porphyroblasts growth was inferred to reflect prograde conditions during crenulation cleavage development and granite emplacement (Reinhardt & Rubenach, 1989). These interpretations implied that the sequence of porphyroblasts observed grew during the same deformation event (D2).

One of the most important and obvious ways to discriminate whether the deformation is progressive or episodic is to determine the age of mineral phases that formed in the axial planar foliations. By combining structural and microstructural criteria with recent geochronology data and P–T estimates, we address this concept in the GTI and summarize the deformation history as follows.

The *first deformation event* (*D1*) in the central domain is preserved by the development of a composite fabric S1, where S1a is defined by ilmenite and quartz inclusion trails in garnet cores (grt_a) and staurolite cores, and S1b is marked by biotite–staurolite rims/staurolite–garnet rims (grt_b)–quartz–muscovite–ilmenite. A combination of Lu-Hf in garnet and U-Pb in monazite geochronology revealed that both syn-S1a garnet (grt_a) and syn-S1b monazite (elongated parallel to S1b) yield a consistent age of circa1600 Ma (Volante et al., 2020). Hence, in the central domain, the first deformation event D1 is characterized by the progressive development of a 1600 Ma composite fabric S1 (i.e., *S1a and S1b*) during garnet and staurolite growth under prograde medium-*P/T* conditions (M1; Figure 12a; Boger & Hansen, 2004; Cihan et al., 2006; Pourteau et al., 2018; Volante et al., 2020).

The D2 deformation event occurred during emplacement of granite sheets in the central domain and partial melting in the eastern domain. In situ U-Pb in monazite grains aligned parallel to S2 constrained the sillimanite–biotite-defining S2 foliation at circa 1550 Ma (M2; Cihan et al., 2006; Volante et al., 2020). The S2 foliation is a composite gneissic to migmatitic fabric formed under *LP/MP–HT* conditions. In the central domain, the transitional stage from the staurolite–garnet D1/M1 peak to the D2/M2 stage is characterized by replacement of andalusite after staurolite. This transitional stage marks an important change in the *P–T* conditions of the system, which reflects decompression and exhumation of the central domain (post-M1; Boger & Hansen, 2004; Cihan et al., 2006; Volante et al., 2020). The early andalusite-bearing *LP–MT* M2a marks the first stages of S2 development (S2a), whereas the *LP–HT* sillimanite-defining M2b mineral assemblage marks the later stages (S2b). In these peak-*T* M2(b) 1550 Ma domains, S2 fabric is the pervasive foliation, with the S1 foliation preserved as quartz-ilmenite inclusion trails in 1600 Ma relict garnet.

Thus, a combination of progressive deformation (e.g., S1a and S1b) within two episodic structural–metamorphic events (e.g., D1, D2) characterized the tectono-thermal evolution of the poly-deformed GTI. This sequence contrasts with the Bell and Rubenach (1983) and Reinhardt and Rubenach (1989) model, which proposed diachronous growth of a porphyroblastic sequence during six stages of progressive development of one dominant deformation (i.e., D2), associated with prograde metamorphism. In contrast, this contribution suggests that the six stages of progressive cleavage development of Bell and Rubenach (1983) occurred twice during two discrete deformation events (i.e., D1 and D2).

5.3. FIAs Analysis Versus Multiscale Petrostructural Approach

The results of our multiscale and multidisciplinary petrostructural and geochronological approach show differences and similarities with the previously suggested structural evolution of the region (e.g., Cihan & Parsons, 2005). In general, studies of FIAs suggest that overprinting fabrics (i.e., inclusions trails) produce unique FIAs in porphyroblasts, the orientation of which allow successive compressive stress fields to be determined (Bell et al., 1995).

The strengths and weaknesses of FIA analysis *versus* a multiscale petrostructural approach are briefly discussed below, on the basis of this study (Tables 1 and 2). Key points of differences between the two approaches in the GTI are as follows:

1. Very few of the FIA trends could be correlated to the regional structures. According to FIA analysis, the E-W folds predated the growth of porphyroblasts in the central domain (Cihan & Parsons, 2005). However, E-W folds formed last and during retrograde metamorphism according to the regional structural analysis (this study). Also, N trending FIA3 axes (ca. 1610–1572 Ma) resemble the circa 1550 Ma N-S trending D2 structures described here. However, the composite S2 fabric is dated at circa 1550 Ma, not circa 1600 Ma. Additionally, the NE-SW FIA4 trend identified only in staurolite porphyroblasts and associated with the development of S3/4 fabric (ca. 1572–1507 Ma; Cihan et al., 2006; Cihan & Parsons, 2005) resembles the NNE-trending D1 structures that are identified by this study and constrained at circa 1600 Ma.

2. Two major deformation events have been recognized in the GTI: D1/M1 at circa 1600 Ma and D2/M2 at circa 1550 Ma. D1/M1 occurred under *MP–MT* conditions, whereas D2/M2 underwent *LP–HT* conditions (Volante et al., 2020). In contrast, FIA studies mainly relate to the circa 1600 Ma deformation event, which occurred at amphibolite-facies conditions in the Grt-St stability field (Cihan & Parsons, 2005).

3. FIA analysis in the GTI was restricted to the central domain, where a D2/M2 high-strain, midcrustal, extensional, ductile shear zone was identified in this study. None of the circa 1550 Ma high-grade deformation events were identified by the FIA analysis nor was the later D3 retrograde event and the NE trending F1 folds in the upper crustal domain. Much of the circa 1550 Ma event was recorded by post andalusite sillimanite growth and migmatization, so it was not captured as porphyroblasts inclusion trails.

4. There is no evidence for the early E-W folds interpreted from FIA analysis (FIA 1–2). If early E-W folds developed, they are not recorded in the upper crustal (western) domain of the GTI. If they did exist, they were confined to the middle crust (5–6 kbar) and the FIA results, at best, highlighted a localized deformational episode. By contrast, the 1600 Ma NE trending F1 folds can be traced several hundred kilometers to the west (Figure 3). The only regional E-W trending folds are associated with the last deformation event during retrograde metamorphism (Volante et al., 2020).

The FIAs method is potentially a valid approach for unraveling the early structural history of a region, because porphyroblasts do not necessarily rotate as the surrounding matrix progressively deforms (e.g., Fay et al., 2008). This phenomenon, known as gyrostasis, occurs because the porphyroblasts can be isolated from the embedding matrix by anastomosing microshear zones that continue to deform noncoaxially as material close to the porphyroblasts continues to deform coaxially (Fay et al., 2008). Also, recent tomographic studies of spiral garnets have confirmed that FIAs do exist in porphyroblasts and can occasionally record successive subvertical and subhorizontal preferred orientations of inclusion trails (Aerden & Ruiz-Fuentes, 2020). This tomographic analysis further supports the interpretation that orogens may undergo alternating phases of crustal shortening and gravitational collapse (cf. Bell & Johnson, 1989).

However, our regional structural analysis of the GTI illustrates some limitations of the FIA approach. This comparison is possible because the GTI is a tilted crustal section, where rocks that formed at circa 1550 Ma span a pressure range corresponding to "paleodepths" of 0–30 km. The "at surface" exposures are represented by the circa 1550 Ma Croydon volcanic rocks directly overlying circa 1650 Ma supracrustal sequences, whereas the eastern domain records peak pressure of ~8 kbar (Volante et al., 2020).

The complex structural history suggested by FIAs in the GTI (i.e., early E-W FIA 1–2), points to midcrustal but no regional upper crustal deformation. If the FIA analysis is accepted, the contrast between the circa 1600 Ma regional upper crustal and apparent mid-crustal structures evident from FIA analysis suggest
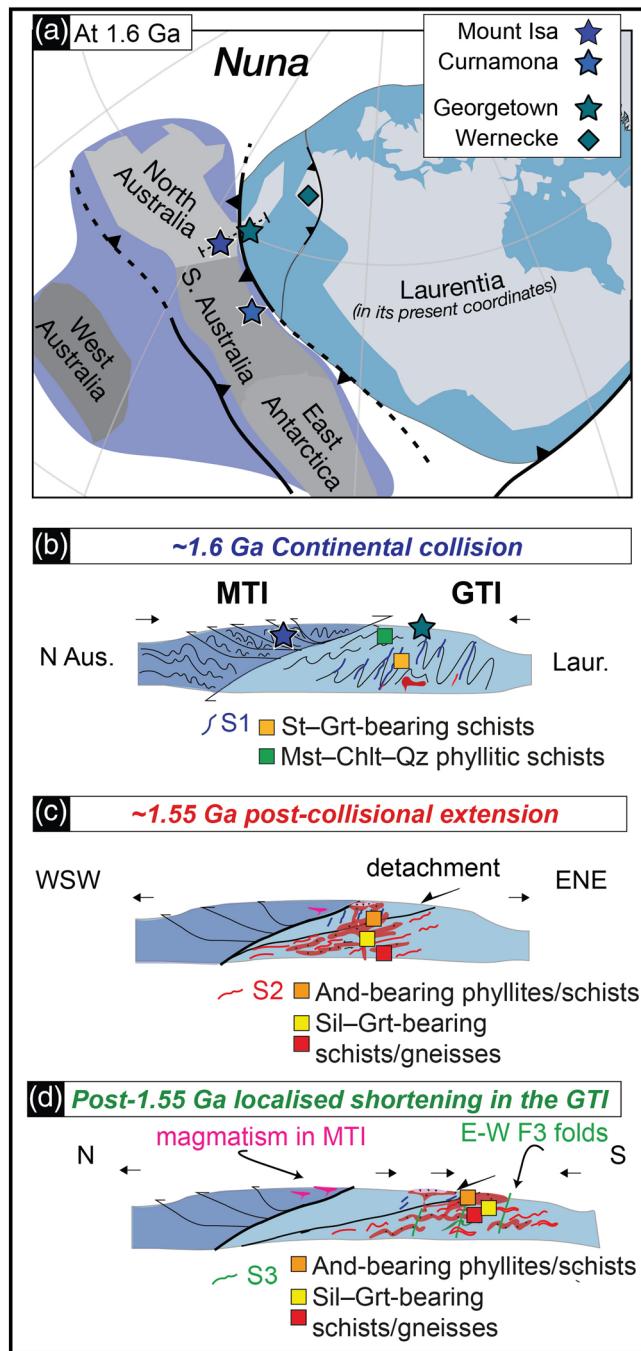
Figure 13. NE Australia during the final assembly of the supercontinent Nuna. (a) Possible Nuna Australia-Antarctica-Laurentia configuration at 1.6 Ga marking the final supercontinent assembly. Modified after Pourteau et al. (2018). Presently emerged continents are shown with their possible original extensions (faded colors). (b) Interpreted schematic crustal section of the 1.60 Ga collisional orogen between Laurentian (Laur.) Georgetown Inlier (GTI) and the eastern North-Australian (N Aus.) Mount Isa Inlier (MTI). (c) Interpreted schematic crustal section of the 1.55 Ga post-collisional extensional event.

that the two crustal domains were decoupled from one another as they deformed. Moreover, the apparent complex deformation recorded by the amphibolite facies circa 1600 Ma porphyroblasts was rapid, all occurring within a relatively short temporal window of prograde garnet and staurolite growth (Cihan et al., 2006). This suggests that the stress field can rapidly change during deformation, but the change is only recorded in the rheologically weak crust forming under prograde amphibolite facies conditions, possibly close to the partial melting threshold when migmatites form. Thus, such rheologically weak zones where FIAs developed may be sensitive recorders of stress field variation, which may not have regional structural significance.

We suggest that a multidisciplinary and multiscale petrostructural analysis at different crustal levels is required to fully understand the tectono-metamorphic evolution of a poly-deformed terrane. Initially, this may seem impractical, however, most orogens are features that extend for hundreds of kilometers and are variably exhumed, so the aim should be to choose regions that record different *P–T* conditions and determine if the age of porphyroblasts growth can be correlated with known structural events in other regions, particularly lower grade structural zones. Then, FIA analysis from amphibolite facies domains might be correlated with higher and lower metamorphic grade domains and the entire structural evolution of orogen can be unraveled.

5.4. Tectono-Metamorphic Domains of the 1600 Ma Orogeny

The progressive variation in metamorphic conditions during polyphase deformation produced distinct textural relationships between the successive foliation generations. We infer that the circa 1600 Ma D1 N-S striking compressional structures are dominant in the western domain, whereas the circa 1550 Ma D2 extensional structures and the *LP–MT/HT* metamorphic overprint are dominant in the central and eastern domains. During this stage, middle- to lower-crustal levels (i.e., core complex) were partially exhumed by a crustal-scale ESE-WNW, top-to-the-west transtensional detachment fault to upper crustal levels. The D2/M2 stage was related to post-collisional extension and synchronous generation of extensive partial melting in the deep crust and voluminous granitic plutons at midcrustal levels, with only minor plutons having reached upper crustal levels in the western domain. In the neighboring MTI, synchronous (1550–1490 Ma), *LP–HT* metamorphism and widespread magmatism (e.g., Mark, 2001; Sayab, 2006) was recorded during progressive and protracted extension (e.g., Blenkinsop, 2005). By contrast, post-1550 Ma retrograde, D3 N-S shortening evidenced in the GTI by conspicuous E-W trending compressional F3 folds (Figure 13d) was not as pervasive in the nearby MTI (e.g., Rubenach et al., 2008).

The poly-deformed GTI, therefore, preserves different stages of the Mesoproterozoic orogenesis related to the final assembly of the supercontinent Nuna at 1600 Ma (Figure 13). Exhumation of ~30 km (0–9 kbar) of crust was accommodated by asymmetric D2 extensional detachment zone, which juxtaposed the 1600 Ma medium-*P/T* compression-related fabrics of the central domain against the 1600 Ma structures in the upper-crustal western domain. This extensional shear zone also exhumed the dominant circa 1550 Ma *LP–HT* S2 foliation and associated extensive syn-D2 granitic sheets of the central domain.

Consequently, the view of a single structural and metamorphic unit is here also questioned. The western, central, and eastern metamorphic domains reflect two tectonic units, where a crustal-scale detachment zone juxtaposed the western to the central and eastern domains. No structural break was identified between the central domain and the eastern migmatitic complex due to the presence of the younger Jurassic and Triassic Newcastle Range cover. For this reason, we can argue for the existence of at least two tectono-metamorphic units: the upper-crustal domain in the west and the exhumed middle- to lower-crustal unit in the central and eastern inlier (Figures 3 and 12).

5.5. Implications of the GTI 1.6 Ga Orogeny During Nuna Final Assembly

Recent metamorphic, structural, and geochronological studies in the GTI have supported the circa 1600 Ma continental collision with the adjacent MTI during Nuna amalgamation previously proposed (Betts et al., 2006, 2011; Gibson et al., 2020; Nordsvan et al., 2018; Pourteau et al., 2018; Volante et al., 2020). Collision is associated with WNW-ESE directed shortening (D1/M1), followed by a WNW-ESE directed extension (D2/M2) at circa 1550 Ma (Volante et al., 2020). Seismic-reflection imaging of the concealed basement between the GTI and MTI (Korsch et al., 2012) suggests an asymmetrical, bivergent thrust wedge, with the possible former plate boundary projecting to the surface undercover between the MTI and the GTI (Pourteau et al., 2018). The crustal architecture of northeastern Australia, typical of collisional orogens (Jamieson & Beaumont, 2013), was interpreted with the GTI as the westward underplating leading edge of Laurentia at 1600 Ma and the MTI as the overriding North Australian plate (e.g., Pourteau et al., 2018).

The circa 1550 Ma low-P/T extensional event now unraveled in the GTI (Cihan et al., 2006; Volante et al., 2020) and in the MTI (Betts et al., 2006; Blenkinsop, 2005) is also consistent with coeval incipient extension documented in western Laurentia (e.g., Pehrsson et al., 2016), supporting the interpreted Australia-Laurentia connection in Nuna.

This region-scale switch from collision to extension suggest a dramatic tectonic reorganization of the final Nuna suture zone, either through slab break off, driving isostatic rebound and development of crustal-scale detachment systems (e.g., Goscombe et al., 2018) or slab roll-back and plate boundary migration (e.g., Collins et al., 2016; Jolivet & Brun, 2010) or orogenic collapse induced by lithospheric delamination (e.g., Li et al., 2010). Soon after the 1550 Ma extensional phase, the GTI underwent N-S shortening (D3) associated with exhumation of the whole terrane under greenschist to lower amphibolite conditions in the western, central and eastern domains, respectively. This retrograde post-1550 Ma event in the GTI was related to extensive hydrothermal activity, possibly linked to the late stages of magmatism and high-temperature metamorphism, along minor and major reactivated shear zones (Hills, 2003), and it was contemporary with continuous magmatic activity in the neighboring MTI until circa 1500 Ma (e.g., Page & Sun, 1998).

6. Conclusions

Understanding the deformation history of poly-deformed terranes requires detailed multiscale investigations. In this contribution, by utilizing such approach with constraints from previously reported geochronology in the Palaeo-Mesoproterozoic GTI (Volante et al., 2020), we report the following statements:

1. The 1600 Ma deformation event D1 developed compressional structures identified in the western domain, where upright F1 folds preserved NNE trending orientation and a steep, E dipping S1 axial planar fabric defined by greenschist facies mineral assemblages. Whereas in the central domain, S1 is a composite fabric (e.g., S1a and S1b) which developed under medium-amphibolite facies conditions and is preserved within S2 low strain domains. D1 compressional structures are related to circa 1600 Ma E-W shortening during continental collision of the Laurentian GTI with the North-Australian MTI during the final assembly of Nuna (Nordsvan et al., 2018; Pourteau et al., 2018).

2. D2 structures in the central and eastern domains are isoclinal and recumbent F2 folds in the footwall of a crustal-scale N-S striking, shallowly W dipping detachment zone. The latter coincides with the *LP–HT* S2 foliation, which developed synchronously with S-type granites emplacement and partial melting. The central and eastern domains reflect exhumed middle- and lower-crustal levels within a circa 1550 Ma D2/M2 extensional detachment zone. The D2/M2 thermal event (e.g., Volante et al., 2020) is associated with post-collisional ESE-WNW, top-to-the-west transtensional movement accommodated by a crustal-scale N-S trending detachment zone and extensive magmatic activity in NE Australia.

3. The latest D3 event produced regional E-W trending upright F3 folds and a steep, retrograde axial planar cleavage S3. During this stage, peak mineral assemblages were variably replaced by lower amphibolite to greenschist facies mineral assemblages. D3 is heterogeneously partitioned with higher strain domains along kilometer-scale F3 limbs and lower strain zones within F3 hinges. D3 occurred during regional N-S shortening post-1550 Ma.

4. In the GTI, composite fabrics developed during three discrete regional events. D1 was associated with the development of a composite foliation S1 (i.e., S1a and S1b) during prograde garnet and staurolite growth. During D2 a progressive composite *LP–MT/HT* and *MP–HT* gneissic S2 foliation is defined by andalusite (S2a) in the early stages and sillimanite (S2b) during the late stages. During the retrograde D3 event (ca. 1540 Ma) a single steep compressional fabric developed (S3) under lower amphibolite to greenschist facies conditions.

5. The use of the FIA approach has to be combined with structural and petrographic observations at different scales, within a wide study area, as well as metamorphic petrology and geochronology to constrain the tectono-metamorphic evolution of poly-deformed and metamorphosed terrains. Accordingly, a multidisciplinary and multiscale approach, where precise multimethod geochronology is applied to superimposed complex fabrics, is necessary to better constraint and correlate macroscale to microscale evolving structures.

6. Circa 1600 Ma burial and crustal thickening in the NE Australian E-W bivergent orogen is associated with the final assembly of the supercontinent Nuna. Postcollisional extension along similar E-W stress field is related to the development of a crustal-scale detachment zone (including complex ductile structures and abundant granitic melt segregation) in the Laurentian lower plate.

Data Availability Statement

Data for this research are described in this paper and included in the following references: Volante et al. (2020), Bell and Rubenach (1983), Hills (2003), Cihan (2004), and Cihan and Parsons (2005).

References

Aerden, D. G. A. M., & Ruiz-Fuentes, A. (2020). X-ray computed micro-tomography of spiral garnets: A new test of how they form. *Journal of Structural Geology*, *136*, 104054. https://doi.org/10.1016/j.jsg.2020.104054

Bain, J. H. C., & Draper, J. J. (Eds.) (1997). *North Queensland Geology* (Vol. 240, p. 600). Brisbane: Australian Geological Survey Organisation/Queensland Department of Mines & Energy Geology, Bulletin.

Bain, J. H. C., Withnall, I. W., Oversby, B. S., & Mackenzie, D. E. (1985). Geology of the Georgetown Region, Queensland. Australian Bureau of Mineral Resources Canberra, ACT, scale 1:250,000.

Baker, M. J., Crawford, A. J., & Withnall, I. W. (2010). Geochemical, Sm–Nd isotopic characteristics and petrogenesis of Paleoproterozoic mafic rocks from the Georgetown Inlier, north Queensland: Implications for relationship with the Broken Hill and Mount Isa Eastern Succession. *Precambrian Research*, *177*(1–2), 39–54. https://doi.org/10.1016/j.precamres.2009.11.003

Bell, T. H. (1978). Progressive deformation and reorientation of fold axes in a ductile mylonite zone: The Woodroffe thrust. *Tectonophysics*, *44*(1–4), 285–320. https://doi.org/10.1016/0040-1951(78)90074-4

Bell, T. H. (1981). Foliation development: The contribution, geometry and significance of progressive bulk inhomogeneous shortening. *Tectonophysics*, *75*(3–4), 273–296. https://doi.org/10.1016/0040-1951(81)90278-X

Bell, T. H. (1986). Foliation development and refraction in metamorphic rocks: Reactivation of earlier foliations and decrenulation due to shifting patterns of deformation partitioning. *Journal of Metamorphic Geology*, *4*(4), 421–444. https://doi.org/10.1111/j.1525-1314.1986.tb00362.x

Bell, T. H., Forde, A., & Wang, J. (1995). A new indicator of movement direction during orogenesis: Measurement technique and application to the Alps. *Terra Nova*, *7*(5), 500–508. https://doi.org/10.1111/j.1365-3121.1995.tb00551.x

Bell, T. H., & Hobbs, B. E. (2010). Foliations and shear sense: A modern approach to an old problem. *Journal of the Geological Society of India*, *75*(1), 137–151. https://doi.org/10.1007/s12594-010-0003-2

Bell, T. H., & Johnson, S. E. (1989). Porphyroblast inclusion trails: The key to orogenesis. *Journal of Metamorphic Geology*, *7*(3), 279–310. https://doi.org/10.1111/j.1525-1314.1989.tb00598.x

Bell, T. H., & Rubenach, M. J. (1980). Crenulation cleavage development—Evidence for progressive bulk inhomogeneous shortening from "millipede" microstructures in the Robertson River Metamorphics. *Tectonophysics*, *68*(1–2), T9–T15. https://doi.org/10.1016/0040-1951(80)90003-7

Bell, T. H., & Rubenach, M. J. (1983). Sequential porphyroblast growth and crenulation cleavage development during progressive deformation. *Tectonophysics*, *92*(1–3), 171–194. https://doi.org/10.1016/0040-1951(83)90089-6

Bell, T. H., Rubenach, M. J., & Fleming, P. D. (1986). Porphyroblast nucleation, growth and dissolution in regional metamorphic rocks as a function of deformation partitioning during foliation development. *Journal of Metamorphic Geology*, *4*(1), 37–67. https://doi.org/10.1111/j.1525-1314.1986.tb00337.x

Betts, P. G., Armit, R. J., Stewart, J., Aitken, A. R. A., Ailleres, L., Donchak, P., et al. (2016). Australia and Nuna. *Geological Society, London, Special Publications*, *424*(1), 47–81. https://doi.org/10.1144/SP424.2

Betts, P. G., Giles, D., & Aitken, A. (2011). Palaeoproterozoic accretion processes of Australia and comparisons with Laurentia. *International Geology Review*, *53*(11–12), 1357–1376. https://doi.org/10.1080/00206814.2010.527646

Betts, P. G., Giles, D., Mark, G., Lister, G. S., Goleby, B. R., & Aillères, L. (2006). Synthesis of the Proterozoic evolution of the Mt Isa Inlier. *Australian Journal of Earth Sciences*, *53*(1), 187–211. https://doi.org/10.1080/08120090500434625

Black, L. P., Bell, T. H., Rubenach, M. J., & Withnall, I. W. (1979). Geochronology of discrete structural-metamorphic events in a multiply deformed Precambrian terrain. *Tectonophysics*, *54*(1–2), 103–137. https://doi.org/10.1016/0040-1951(79)90114-8

Black, L. P., Gregory, P., Withnall, I. W., & Bain, J. H. C. (1998). U-Pb zircon age for the Etheridge Group, Georgetown region, north Queensland: Implications for relationship with the Broken Hill and Mt Isa sequences. *Australian Journal of Earth Sciences*, *45*(6), 925–935. https://doi.org/10.1080/08120099808728446

Black, L. P., & McCulloch, M. T. (1990). Isotopic evidence for the dependence of recurrent felsic magmatism on new crust formation: An example from the Georgetown region of northeastern Australia. *Geochimica et Cosmochimica Acta*, *54*(1), 183–196. https://doi.org/10.1016/0016-7037(90)90206-Z

Black, L. P., & Withnall, I. W. (1993). The ages of Proterozoic granites in the Georgetown inlier of northeastern Australia, and their relevance to the dating of tectonothermal events. *AGSO Journal of Australian Geology and Geophysics*, *14*, 331–341.

Black, L. P., Withnall, I. W., Gregory, P., Oversby, B. S., & Bain, J. H. C. (2005). U-Pb zircon ages from leucogneiss in the Etheridge Group and their significance for the early history of the Georgetown region, north Queensland. *Australian Journal of Earth Sciences*, *52*(3), 385–401. https://doi.org/10.1080/08120090500134522

Blenkinsop, T. G. (2005). *Total Systems Analysis of the Mount Isa Eastern Succession*. Report. Predictive Mineral Discovery CRC.

Boger, S. D., & Hansen, D. (2004). Metamorphic evolution of the Georgetown Inlier, northeast Queensland, Australia; evidence for an accreted Palaeoproterozoic terrane? *Journal of Metamorphic Geology*, *22*(6), 511–527. https://doi.org/10.1111/j.1525-1314.2004.00528.x

Cihan, M. (2004). The drawbacks of sectioning rocks relative to fabric orientations in the matrix: A case study from the Robertson River Metamorphics (Northern Queensland, Australia). *Journal of structural Geology*, *26*, 2157–2174. https://doi.org/10.1016/J.JSG.2004.07.001

Cihan, M., Evins, P., Lisowiec, N., & Blake, K. (2006). Time constraints on deformation and metamorphism from EPMA dating of monazite in the Proterozoic Robertson River Metamorphics, NE Australia. *Precambrian Research*, *145*(1–2), 1–23. https://doi.org/10.1016/J.PRECAMRES.2005.11.009

Cihan, M., & Parsons, A. (2005). The use of porphyroblasts to resolve the history of macro-scale structures: An example from the Robertson River Metamorphics, North-eastern Australia. *Journal of Structural Geology*, *27*(6), 1027–1045. https://doi.org/10.1016/j.jsg.2005.02.004

Collins, W. J., Huang, H.-Q., & Jiang, X. (2016). Water-fluxed crustal melting produces Cordilleran batholiths. *Geology*, *44*(2), 143–146. https://doi.org/10.1130/G37398.1

Connors, K. A., & Lister, G. S. (1995). Polyphase deformation in the western Mount Isa Inlier, Australia: Episodic or continuous deformation? *Journal of Structural Geology*, *17*(3), 305–328. https://doi.org/10.1016/0191-8141(94)00057-7

Davis, B. K. (1995). Regional-scale foliation reactivation and re-use during formation of a macroscopic fold in the Robertson River Metamorphics, north Queensland, Australia. *Tectonophysics*, *242*(3–4), 293–311. https://doi.org/10.1016/0040-1951(94)00212-R

Duncan, A. C., & Withnall, I. W. (1983). Definition of the Proterozoic Juntala Metamorphics, Georgetown Inlier, north Queensland. *Queensland Government Mining Journal*, *84*, 191–192.

Fay, C., Bell, T. H., & Hobbs, B. E. (2008). Porphyroblast rotation versus nonrotation: Conflict resolution. *Geology*, *36*(4), 307–310. https://doi.org/10.1130/G24499A.1

Ghosh, S. K., & Sengupta, S. (1987). Progressive development of structures in a ductile shear zone. *Journal of Structural Geology*, *9*(3), 277–287. https://doi.org/10.1016/0191-8141(87)90052-6

Gibson, G. M., Champion, D. C., Huston, D. L., & Withnall, I. W. (2020). Orogenesis in Paleo-Mesoproterozoic eastern Australia: A response to arc-continent and continent-continent collision during assembly of the Nuna Supercontinent. *Tectonics*, e21241. https://doi.org/10.1029/2019TC005717

Goscombe, B., Gray, D., & Foster, D. A. (2018). Metamorphic response to collision in the Central Himalayan Orogen. *Gondwana Research*, *57*, 191–265. https://doi.org/10.1016/j.gr.2018.02.002

Gosso, G., Rebay, G., Roda, M., Spalla, M. I., Tarallo, M., Zanoni, D., & Zucali, M. (2015). Taking advantage of petrostructural heterogeneities in subduction-collisional orogens, and effect on the scale of analysis. *Periodico di Mineralogia*, *84*, 779–825. https://doi.org/10.2451/2015PM0452

Hayward, N. (1990). Determination of early fold axis orientations in multiply deformed rocks using porphyroblast inclusion trails. *Tectonophysics*, *179*(3–4), 353–369. https://doi.org/10.1016/0040-1951(90)90301-N

Hills, Q. (2003). Deformational and metamorphic history of the Georgetown Inlier, north Queensland implications for the 1.7 to 1.5 Ga tectonic evolution of northeastern Proterozoic Australia (PhD thesis). (Retrieved from https://bridges.monash.edu/articles/The_deformational_and_metamorphic_history_of_the_Georgetown_Inlier_North_Queensland_implications_for_the_1_7_to_1_5_Ga_tectonic_evolution_of_northeastern_Proterozoic_Australia/4633945). Monash University, 2004.

Hobbs, B. E., Means, W. D., & Williams, P. F. (1976). *An outline of structural geology* (p. 571). New York: Wiley.

Holdsworth, R. E. (1990). Progressive deformation structures associated with ductile thrusts in the Moine Nappe, Sutherland, Scotland. *Journal of Structural Geology*, *12*(4), 443–452. https://doi.org/10.1016/0191-8141(90)90033-U

Holdsworth, R. E., & Roberts, A. M. (1984). Early curvilinear fold structures and strain in the Moine of the Glen Garry region, Inverness-shire. *Journal of the Geological Society*, *141*(2), 327–338. https://doi.org/10.1144/gsjgs.141.2.0327

Jamieson, R. A., & Beaumont, C. (2013). On the origin of orogens. *Geological Society of America Bulletin*, *125*(11–12), 1671–1702. https://doi.org/10.1130/b30855.1

Jolivet, L., & Brun, J.-P. (2010). Cenozoic geodynamic evolution of the Aegean. *International Journal of Earth Sciences*, *99*(1), 109–138. https://doi.org/10.1007/s00531-008-0366-4

Kirscher, U., Liu, Y., Li, Z. X., Mitchell, R. N., Pisarevsky, S. A., Denyszyn, S. W., & Nordsvan, A. (2019). Paleomagnetism of the Hart Dolerite (Kimberley, Western Australia)—A two-stage assembly of the supercontinent Nuna? *Precambrian Research*, *329*, 170–181. https://doi.org/10.1016/j.precamres.2018.12.026

Kirscher, U., Mitchell, R. N., Liu, Y., Nordsvan, A. R., Cox, G. M., Pisarevsky, S. A., et al. (2020). Paleomagnetic constraints on the duration of the Australia-Laurentia connection in the core of the Nuna supercontinent. *Geology*, https://doi.org/10.1130/G47823.1

Korsch, R. J., Huston, D. L., Henderson, R. A., Blewett, R. S., Withnall, I. W., Fergusson, C. L., et al. (2012). Crustal architecture and geodynamics of North Queensland, Australia: Insights from deep seismic reflection profiling. *Tectonophysics*, *572–573*, 76–99. https://doi.org/10.1016/j.tecto.2012.02.022

Li, Z.-X., Li, X.-H., Wartho, J.-A., Clark, C., Li, W.-X., Zhang, C.-L., & Bao, C. (2010). Magmatic and metamorphic events during the early Paleozoic Wuyi-Yunkai orogeny, southeastern South China: New age constraints and pressure-temperature conditions. *Bulletin*, *122*(5–6), 772–793. https://doi.org/10.1130/b30021.1

Mark, G. (2001). Nd isotope and petrogenetic constraints for the origin of the Mount Angelay igneous complex: Implications for the origin of intrusions in the Cloncurry district, NE Australia. *Precambrian Research*, *105*(1), 17–35. https://doi.org/10.1016/S0301-9268(00)00101-7

Neumann, N. L., & Kositcin, N. (2011). New SHRIMP U-Pb zircon ages from North Queensland, 2007–2010. Geoscience Australia Record, 2011/38.

Nordsvan, A. R., Collins, W. J., Li, Z.-X., Spencer, C. J., Pourteau, A., Withnall, I. W., et al. (2018). Laurentian crust in northeast Australia: Implications for the assembly of the supercontinent Nuna. *Geology*, *46*(3), 251–254. https://doi.org/10.1130/G39980.1

Page, R. W., & Sun, S. S. (1998). Aspects of geochronology and crustal evolution in the Eastern Fold Belt, Mt Isa Inlier. *Australian Journal of Earth Sciences*, *45*(3), 343–361. https://doi.org/10.1080/08120099808728396

Passchier, C. W. (1990). Reconstruction of deformation and flow parameters from deformed vein sets. *Tectonophysics*, *180*(2–4), 185–199. https://doi.org/10.1016/0040-1951(90)90307-T

Passchier, C. W., & Trouw, R. A. J. (2005). *Microtectonics* (2nd, Revis ed.). New York: Springer Berlin Heidelberg.

Pehrsson, S. J., Eglington, B. M., Evans, D. A. D., Huston, D., & Reddy, S. M. (2016). *Metallogeny and its link to orogenic style during the Nuna supercontinent cycle*, *Special Publications* (Vol. 424, pp. 83–94). London: Geological Society. https://doi.org/10.1144/SP424.5

Pisarevsky, S. A., Elming, S.-Å., Pesonen, L. J., & Li, Z.-X. (2014). Mesoproterozoic paleogeography: Supercontinent and beyond. *Precambrian Research*, *244*, 207–225. https://doi.org/10.1016/j.precamres.2013.05.014

Platt, J. P. (1993). Exhumation of high-pressure rocks: A review of concepts and processes. *Terra Nova*, *5*(2), 119–133. https://doi.org/10.1111/j.1365-3121.1993.tb00237.x

Pourteau, A., Doucet, L. S., Blereau, E. R., Volante, S., Johnson, T. E., Collins, W. J., et al. (2020). TTG generation by fluid-fluxed crustal melting: Direct evidence from the Proterozoic Georgetown Inlier, NE Australia. *Earth and Planetary Science Letters*, *550*, 116548. https://doi.org/10.1016/j.epsl.2020.116548

Pourteau, A., Smit, M. A., Li, Z.-X., Collins, W. J., Nordsvan, A. R., Volante, S., & Li, J. (2018). 1.6 Ga crustal thickening along the final Nuna suture. *Geology*, *46*(11), 959–962. https://doi.org/10.1130/G45198.1

Ramsay, J. G. (1967). *Folding and Fracturing of Rocks*. New York: McGraw-Hill.

Reinhardt, J., & Rubenach, M. J. (1989). Temperature-time relationships across metamorphic zones: Evidence from porphyroblast—Matrix relationships in progressively deformed metapelites. *Tectonophysics*, *158*(1–4), 141–161. https://doi.org/10.1016/0040-1951(89)90321-1

Rubenach, M. J., Foster, D. R. W., Evins, P. M., Blake, K. L., & Fanning, C. M. (2008). Age constraints on the tectonothermal evolution of the Selwyn Zone, Eastern fold belt, Mount Isa Inlier. *Precambrian Research*, *163*(1–2), 81–107. https://doi.org/10.1016/j.precamres.2007.08.014

Sawyer, E. W. (2008). *Atlas of Migmatites*, *Special Publication* (Vol. 9). Ottawa, Ontario, Canada: Mineralogical Association of Canada. https://doi.org/10.1139/9780660197876

Sayab, M. (2006). Decompression through clockwise P–T path: Implications for early N–S shortening orogenesis in the Mesoproterozoic Mt Isa Inlier (NE Australia). *Journal of Metamorphic Geology*, *24*(2), 89–105. https://doi.org/10.1111/j.1525-1314.2005.00626.x

SeyİToĞLu, G., & Veysel, I. (2015). Late Cenozoic extensional tectonics in western Anatolia: Exhumation of the Menderes core complex and formation of related basins. *Maden Tetkik ve Arama Dergisi*, *151*(151), 47–106. https://doi.org/10.19111/bmre.49951

Spalla, M. I., Siletto, G. B., di Paola, S., & Gosso, G. (2000). The role of structural and metamorphic memory in the distinction of tectono-metamorphic units: The basement of the Como lake in the Southern Alps. *Journal of Geodynamics*, *30*(1-2), 191–204. https://doi.org/10.1016/S0264-3707(99)00033-2

Tobisch, O. T., & Paterson, S. R. (1988). Analysis and interpretation of composite foliations in areas of progressive deformation. *Journal of Structural Geology*, *10*(7), 745–754. https://doi.org/10.1016/0191-8141(88)90081-8

Volante, S., Pourteau, A., Collins, W. J., Blereau, E., Li, Z.-X., Smit, M., et al. (2020). Multiple P–T–d–t paths reveal the evolution of the final Nuna assembly in northeast Australia. *Journal of Metamorphic Geology*, *38*(6), 593–627. https://doi.org/10.1111/jmg.12532

Whitney, D. L., & Evans, B. W. (2010). Abbreviations for names of rock-forming minerals. *American Mineralogist*, *95*(1), 185–187. https://doi.org/10.2138/am.2010.3371

Williams, P. F. (1967). Structural analysis of the Little Broken Hill area, New South Wales. *Journal of the Geological Society of Australia*, *14*(2), 317–331. https://doi.org/10.1080/00167616708728669

Williams, P. F. (1985). Multiply deformed terrains—Problems of correlation. *Journal of Structural Geology*, *7*(3–4), 269–280. https://doi.org/10.1016/0191-8141(85)90035-5

Williams, P. F., & Zwart, H. J. (1977). A model for the development of the Seve-Koeli Caledonian nappe complex. In *Energetics of geological processes* (pp. 169–187). New York: Springer.

Withnall, I. W. (1985). Geochemistry and tectonic significance of Proterozoic rocks from the Georgetown Inlier, north Queensland Bureau of Mineral Resources. *Journal of Australian Geology and Geophysics*, *9*, 339–351.

Withnall, I. W. (1996). Stratigraphy, Structure and Metamorphism of the Proterozoic Etheridge and Langlovale Groups, Georgetown Inlier, North Queensland. Australian Geological Survey Organisation.

Withnall, I. W., Bain, J. H. C., Draper, J. J., MacKenzie, D. E., & Oversby, B. S. (1988). Proterozoic stratigraphy and tectonic history of the Georgetown Inlier, northeastern Queensland. *Precambrian Research*, *40*(41), 429–446. https://doi.org/10.1016/0301-9268(88)90079-4

Withnall, I. W., & Henderson, R. A. (2012). Accretion on the long-lived continental margin of northeastern Australia. *Episodes*, *35*(1), 166–176. https://doi.org/10.18814/epiiugs/2012/v35i1/016

Withnall, I. W., & Hutton, L. J. (2013). Chapter 2 North Australian Craton. In P. A. Jell (Ed.), *Geology of Queensland* (pp. 23–112). Queensland: Department of Natural Resources and Mines.

Withnall, I. W., Hutton, L. J., Armit, R. J., Betts, P. G., Blewett, R. S., Champion, D. C., & Jell, P. A. (2013). North Australian Craton. In *Geology of Queensland* (pp. 23–112). Queensland: Geological Survey of Queensland.

Withnall, I. W., & Mackenzie, D. E. (1980). New and revised stratigraphic units in the Proterozoic Georgetown Inlier, north Queensland. *Queensland Government Mining Journal*, *81*, 28–43.

Zucali, M., Spalla, M. I., & Gosso, G. (2002). Strain partitioning and fabric evolution as a correlation tool: The example of the Eclogitic Micaschists Complex in the Sesia-Lanzo Zone (Monte Mucrone-Monte Mars, Western Alps, Italy). *Schweizerische Mineralogische und Petrographische Mitteilungen*, *82*(3), 429–454.

Zwart, H. J. (1962). On the determination of polymetamorphic mineral associations, and its application to the Bosost area (central Pyrenees). *Geologische Rundschau*, *52*(1), 38–65. https://doi.org/10.1007/BF01840064